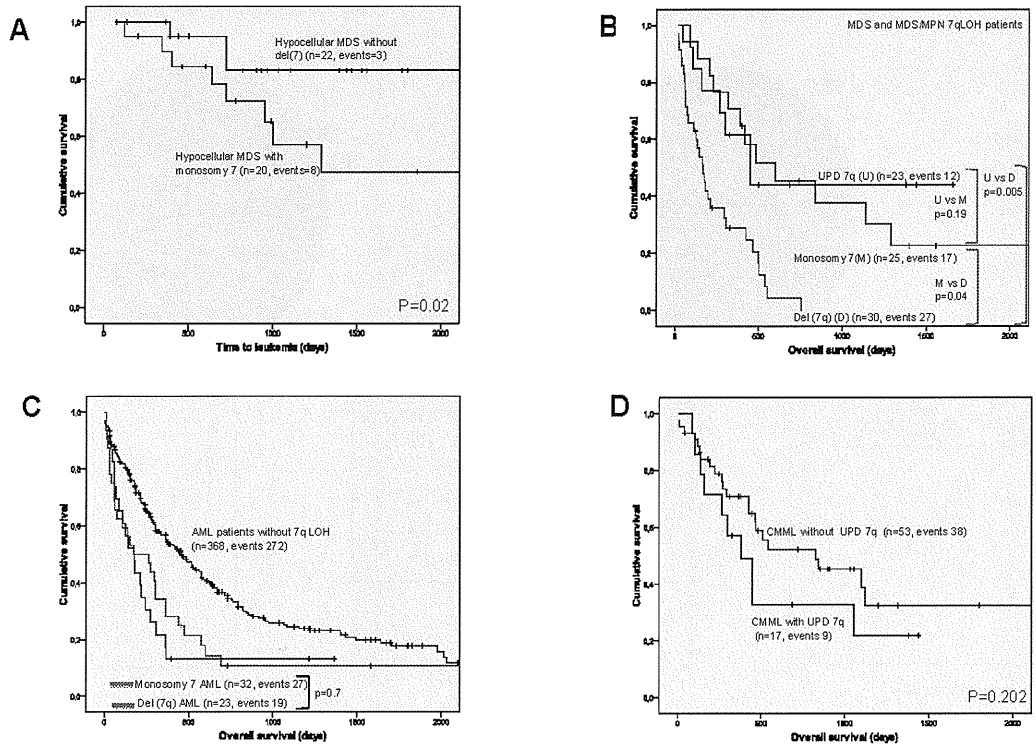

Figure 3. Differences in survival outcomes and progression-free survival of 7q LOH patients. *P* values presented correspond to the Cox regression between the groups indicated. AML indicates acute myeloid leukemia; Chr, chromosome, MDS/MPN, myelodysplastic syndrome/myeloproliferative neoplasm; UPD, uniparental disomy; monosomy 7, deletion of whole chromosome 7; del(7q), partial deletion involving 7q; and CMML, chronic myeloid leukemia.

There are 2 main limitations of SNP-A relative to MC: SNP-A does not detect balanced translocations and SNP-A cannot distinguish whether multiple abnormalities exist in a single clone. We tested whether both techniques could complement each other to solve these shortcomings. We grouped patients based on the presence of monosomy 7/del(7q) in less than 100% or in 100% of the metaphases analyzed. Patients with a clone burden of 100% had a lower median OS (175 vs 235 days; $P = .150$), probably because of the presence of more patients with MDS-derived AML (12 vs 6 cases; $P = .103$), although neither of these findings reached statistical significance. Regarding balanced rearrangements, they were present in 28% of patients, included in complex karyotypes with 5 or more abnormalities in all cases except for 1 patient with a del(7q) and an inv(3)(q21q26). The latter was the only recurrent balanced rearrangement, present in a second patient. The accumulation of this balanced aberrations patients with complex karyotypes and more than 10% of blasts explains partly why the presence of balanced rearrangements did not add independent prognostic value when 1 of those 2 variables was tested simultaneously

Exploring the 2-hit model: SNP-A definition of CDRs and NGS approach

To determine the location of genes on 7q that may be involved in clonal hematopoiesis, we analyzed the SNP-A karyotyping results from 161 patients and defined 3 CDRs, localized in bands 7q22 (100634238-101658775), 7q34 (137841484-139319208), and between bands 7q35 and 7q36.1 (144338001-148572945, Figure 4A). Genomic annotation of the CDRs was performed, and several candidate genes mapping within the CDR were noted (Figure 5); these genes were Sanger sequenced in a cohort of 50 cases with 7q LOH. The third CDR was defined by a single patient with a small deletion containing 6 genes. We sequenced all exons of these genes and detected a mutation in *EZH2*, located in exon 19 involving position Ile715, that produced a frameshift mutation. We found no

Table 2. Multivariate Cox proportional hazards regression models testing the prognostic value of SNP-A chromosome 7 findings in MDS and CMML

MDS multivariate Cox model (n = 274)			CMML multivariate Cox model (n = 70)		
	P	HR (95% CI)		*P*	HR (95% CI)
BM blasts*	≤ .001	1.8 (1.3-2.4)	BM blasts > 10%	.01	10.4 (2.6-41.4)
Presence of blasts in PB	.01	10.3 (2.5-42.2)			
No. of cytopenias†	.13	1.7 (0.8-3.4)	Lymphocyte count > 2.5 × 10^9/L	.6	0.7 (0.2-2.7)
7q LOH SNP-A category‡	≤ .001	4.5 (3.1-6.7)	Hemoglobin level < 12 g/dL	.4	1.7 (0.4-8)
Presence of a UPD(7q)	.1	4.4 (0.8-16)			

HR indicates hazard ratio; BM, bone marrow; PB, peripheral blood; SNP-A, single nucleotide polymorphism array; and CI, confidence interval.

*Three BM blasts categories according to the percentage described: < 5; 5-10; and 11-20.

†Number of cytopenias categories defined as good (0-1) and poor (2-3). Cytopenias defined as hemoglobin less than 10 g/dL, absolute neutrophil count less than 1.8 × 10^9/L, and platelets less than 100 × 10^9/L.

‡7q LOH SNP-A category defined as good, no deletion; intermediate, monosomy 7; and poor, partial deletion involving 7q.

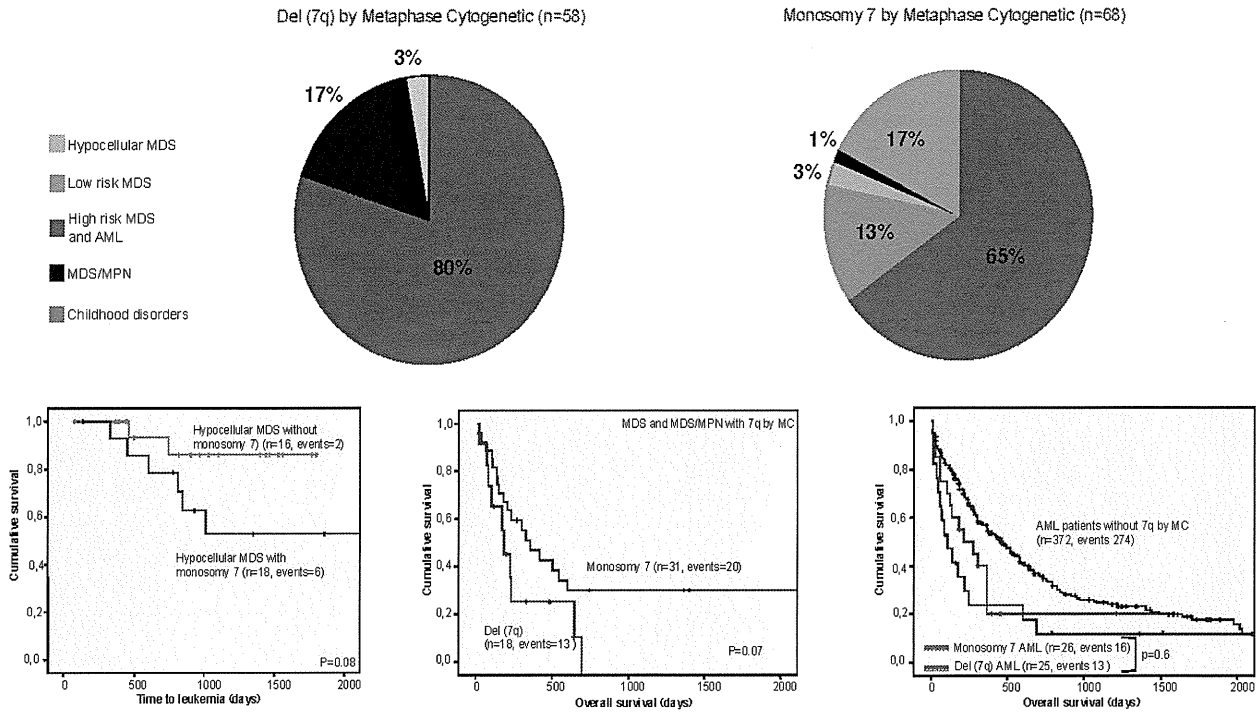

Figure 4. Illustration of how the distribution of disease subsets and outcome associations would be according to the lesion found by MC. (Top) Distribution of patients detected separated according to lesion detected by metaphase cytogenetics. Patients have been grouped as follows: red, AML + high risk and intermediate-2 MDS; gray, low risk and intermediate-1 MDS; blue, hypocellular MDS; black, MDS/MPN; and green, Fanconi anemia and JMML. (Bottom) Differences in survival outcomes and progression-free survival according to MC findings. *P* values presented correspond to the Cox regression between the groups indicated. AML indicates acute myeloid leukemia; Chr, chromosome, MDS/MPN, myelodysplastic syndrome/myeloproliferative neoplasm; UPD, uniparental disomy; monosomy 7, deletion of whole chromosome 7; del(7q), partial deletion involving 7q; and CMML, chronic myeloid leukemia.

other somatic mutations by this strategy. *EZH2* proved to be recurrent in patients with a myelodysplastic/myeloproliferative component and UPD(7q). Supplemental Table 1 summarizes EZH2 mutations found in our 7q LOH patients that we reported previously in part.[20]

In an effort to overcome the limitations inherent to the classic screening method, which was limited to the genes located in the CDRs, we applied 2 NGS approaches. First, we generated exome chromosome 7 libraries from 11 cases with LOH 7q (monosomy 7, n = 6; del(7q), n = 2; UPD(7q), n = 3) and subjected them to

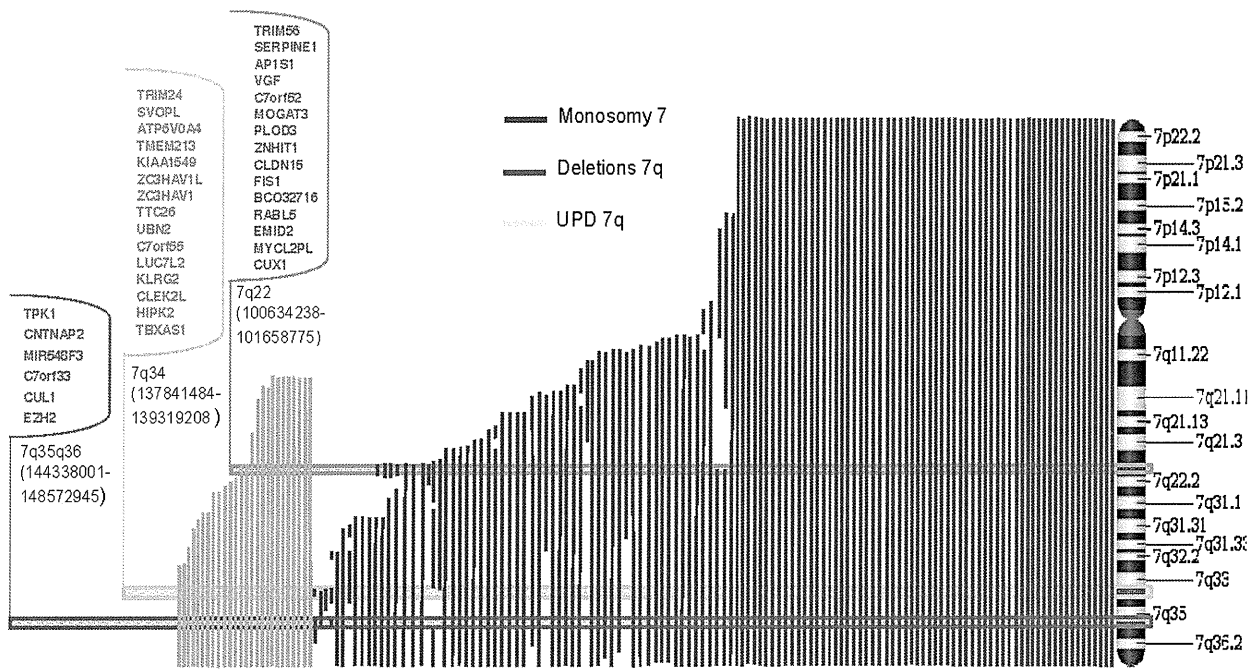

Figure 5. Identification of candidate genes on 7q by mapping CDRs by SNP-A. Three distinct CDRs, indicated by horizontal rectangles, were identified on 7q by mapping of SNP-A karyotyping. The connected keys show the candidate genes contained in each CDR; those genes sequenced in a test cohort of 50 patients with LOH 7q are in bold. CDR indicates commonly deleted region; SNP-A, single nucleotide polymorphism array; and LOH, loss of heterozygosity.

Table 3. Somatic mutations found in regions of 7q LOH patients by NGS

Diagnosis	SNP-A LOH on chromosome 7	Gene	Mutation
MDS/MPN (CMML)	UPD 7q11.21-qter	*EZH2*	R690H
MDS/MPN (aCML)	UPD 7q32.1-qter	*EZH2*	R690H
MDS (RCMD)	Del 7q21.3-qter	*LMTK2A*	A1147T
MDS (RCMD)	Monosomy 7	*NRCAM*	Q1040K
AML	Del 7q21.12q36.3	*ZAN*	N1098Del
AML	Monosomy 7	*GRM8*	A686V
AML	Monosomy 7	*ENSG00000133375*	R68Q
AML	Del 7q31.31-qter	*LOC641808*	V162fs
AML	Monosomy 7	*SEMA3A*	R613Q
AML	Del 7q31.1q36.3	*DYNC1I1*	R239W
AML	Monosomy 7	*HYAL4*	N253K
AML	Monosomy 7	*FAM40B*	C182R
AML	Monosomy 7	*LOC100128744*	P354L
AML	Monosomy 7	*LUC7L2*	R252fs
AML	Del 7q21.11q36.3	*CTAGE6*	T288M
AML	Monosomy 7	*FAM115A*	F193S
AML	Del 7q35-qter	*CUL1*	E241D
AML	Monosomy 7	*EZH2*	E745fs
AML	Del 7q11.21q36.3	*EZH2*	R690H
AML	Monosomy 7	*SSPO*	T426R

SNP-A indicates single nucleotide polymorphism array; LOH, loss of heterozygosity; Del, deletion; MDS/MPN, myelodysplastic syndrome/myeloproliferative neoplasm; CMML, chronic myelomonocytic leukemia; UPD, uniparental disomy; RCMD, refractory cytopenia with multilineage dysplasia; AML, acute myeloid leukemia; and aCML, atypical chronic myelogenous leukemia.

high-throughput sequencing on a Genome Analyzer (Illumina). Second, paired (bone marrow and $CD3^+$) samples from 15 myeloid neoplasms were subjected to whole exome sequencing using HiSeq 2000 (Illumina), including 3 patients with 7q LOH (UPD, deletion, and monosomy). Finally, we used publically available NGS data from TCGA for 74 AML patients. Supplemental Figure 2 shows the somatic mutations found in regions of 7q LOH: *NRCAM* (Q1040K) in a patient with refractory cytopenia with multilineage dysplasia with monosomy 7, *LMTK2* (A1147T) in a refractory cytopenia with multilineage dysplasia patient with del(7q), and *EZH2* (R690H) in a third MDS/MPN patient with UPD(7q). Of note, only mutations of *EZH2* proved to be recurrent [10/19 CMML patients with UPD(7q)], when sequencing by Sanger technique a confirmatory cohort of 50 cases with 7q LOH. Table 3 shows somatic mutations, localized on chromosome 7q, in patients with 7q LOH found using NGS in our patients and in the TCGA project.

Testing the haploinsufficiency hypothesis: microarray expression data

We examined the gene expression profiles of the $CD34^+$ cells of 183 MDS patients, of which 9 cases had monosomy 7 or del(7q). We found that expression of 40% of the genes included in our SNP-A–defined CDRs were significantly reduced in those monosomy 7/del(7q) patients. These genes included *LUC7L2*, *ZNHIT1*, *TTC26*, *RABL5*, *TRIM24*, *EZH2*, *ZC3HAV1L*, *CNTNAP2*, *TRIM24*, *CUX1*, *FIS1*, *RABL5*, *ZC3HAV1*, and *TBXAS1* (supplemental Figure 3). The mean decrease in expression levels was 42% to 33% of that in healthy controls. We also determined the expression of these genes in the 174 cases of MDS that did not have any chromosome 7 deletions, and most interestingly, we found that *EZH2* and *RABL5* were significantly down-regulated even in samples diploid for chromosome 7. Of note, we found that down-regulation of EZH2 was significantly reduced in patients with excess of blasts (Figures 5-6 and supplemental Figure 4).

Discussion

Unlike myeloid disorders harboring an isolated chromosome 5q deletion, a clear genotype-phenotype relationship has not been described in cases with 7q LOH, and underlying pathogenetic mechanisms remain unclear. Here, we applied high-resolution genomic technologies to accurately define the extent and nature of chromosomal lesions and to explore relevant clinical associations of inactivating mutations or insufficient gene dosage in a large cohort of patients with myeloid malignancies involving LOH of the long arm of chromosome 7. Our analyses demonstrate that in those subsets with isolated 7q LOH or accompanied by a very low number of additional lesions, the genotype-phenotype relation is clearly discernible. We found a correlation between an isolated deletion of the long arm of chromosome 7 and MDS with hypoplastic features, and between the presence of UPD(7q) in diploid MDS/MPN patients. In the latter group, the predominant driving genomic event was the presence of inactivating mutations involving *EZH2*, a finding supported by previous studies,[21] whereas gene dosage effect seems to be paramount in typically large monosomy 7/del(7q) cases.

As expected, the spectrum of entities in each 7q LOH subgroup was relatively heterogeneous. Nevertheless, we found strong associations of SNP-A abnormalities with particular clinical entities that merit emphasis. We found a significant association of large MC-cryptic UPD(7q) segments among CMML patients (26%). In our experience, CMML shows a strikingly elevated frequency of somatic UPD compared with other myeloid disorders (data not shown). Particularly high frequencies of somatic UPD have been described for some neoplasms, suggesting that this specific type of chromosomal instability may be related to pathologic pathways that are common in some malignancies but absent in others.[22] In addition, we observed a trend toward worse median survival of CMML patients harboring UPD(7q). The lack of MC lesions in a significant proportion of CMML patients and their controversial

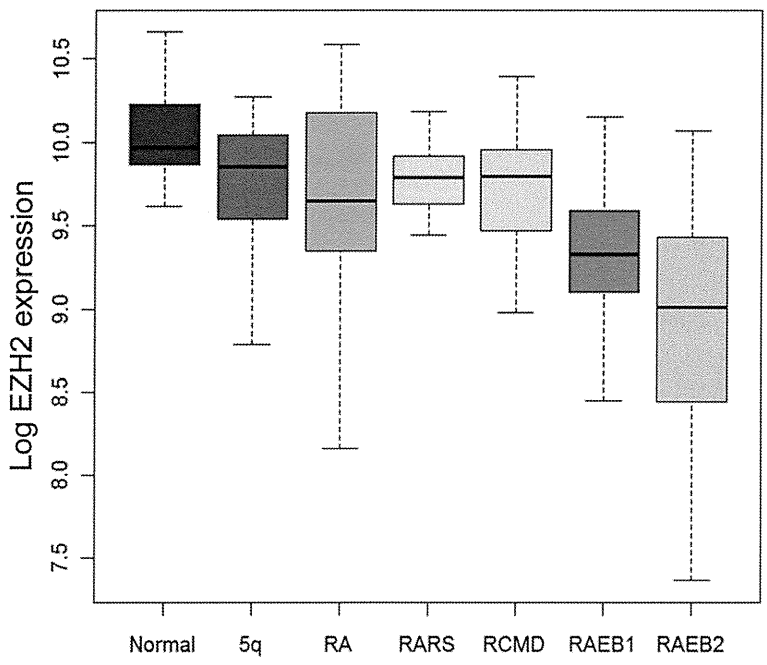

	NML	5q-	RA	RARS	RCMD	RAEB1	RAEB2
Mean	870.668741	839.9296	911.6609	858.685444	880.8111386	654.454716	557.388956
Ttest		0.019892	0.151551	0.00488668	0.004296769	1.0936E-07	2.5564E-09
N	17	17	15	23	43	37	39

Figure 6. Box plots showing the *EZH2* expression ratios obtained in CD34+ cells of 174 MDS cases without 7q LOH and 17 healthy controls. A significant down-regulation of expression was identified for EZH2 in excess of blasts subgroups. NML indicates normal controls; 5q-, 5q-syndrome; RA, refractory anemia; RARS, refractory anemia with ring sideroblasts; RCMD, refractory anemia with multilineage dysplasia; and RAEB, refractory anemia with excess of blasts.

impact on survival,[19,23] increases the value of a possible prognostic significance of UPD(7q).

Hypocellular MDS is a relatively uncommon entity among myeloid disorders, with a possible immune-related pathogenetic component, and a diagnosis that frequently overlaps with aplastic anemia.[24] Within our cohort, 8% of patients had hypocellular MDS, a slightly lower percentage than what has been described in other studies.[25,26] Of note, half of our hMDS cohort harbored monosomy 7 as the sole SNP-A lesion detected, conferring on them a higher rate of leukemia transformation. This finding may be helpful for distinguishing hMDS from other MDS.

The risk group assignment of MDS patients with monosomy 7 has been investigated in several studies.[5,6] These studies reported dissimilar results that could be driven by the difficulty of dissecting, in a highly precise and reproducible way, the karyotype defects by conventional chromosome banding techniques. We and others, using more accurate karyotyping means, showed discrepancies in the context of 5q lesions.[27,28] In our cohort, MDS patients harboring monosomy 7 presented a longer median OS than patients with partial deletions, more closely approximating that reported for the intermediate cytogenetic group in the IPSS.[3] We also showed that the wrong assignment to the monosomy 7 subgroup by MC of a significant number of cases with partial deletions by SNP-A seems to be the responsible of a loss in the prognostic value of the conventional karyotyping technique. The better survival of those patients with a wider loss of genes in chromosome 7 (monosomy 7) than those with partial deletions could be presented as paradoxical. The frequent presence of monosomy 7 either in childhood disorders and not accompanied by other chromosomal lesions on one hand, and the common association of partial deletions of 7 with other chromosomal abnormalities shown to be early events in the genesis of dysplasia [del(5q)] on the other hand,[29,30] prompt us to speculate that monosomy 7 might be a founding genomic aberration and that partial deletions of 7 might represent a secondary event in the context of preexisting genomic instability and therefore within a more aggressive clone.

The large size of the typical chromosomal LOH involving the long arm of chromosome 7 in myeloid disorders has complicated the search for a mutated TSG in this region. In this study, we used 2 approaches: (1) a classic approach with the definition of commonly deleted regions and direct sequencing of candidate genes and (2) a next-generation whole exome strategy. Three SNP-A–defined CDRs were described encompassing, with slight differences, those described previously.[31,32] NGS technology allowed us to cover all coding exons, and because no recurrent mutation other than *EZH2* was found, led us to conclude that the absence of recurrent somatic mutations in patients with monosomy 7/del(7q) is a hallmark of the disease pathogenesis in this unique category of myeloid neoplasms

The lack of recurrent mutations in any of the genes mapping to the segment of LOH in most of the patients with large monosomy 7/del(7q) prompted us to test the haploinsufficiency hypothesis by analyzing the expression profiles of patients with that kind of lesions. The dosage effect resulting from the loss of the whole q arm of chromosome 7 particularly affected genes localized in our 3 CDRs; 14 genes included in our SNP-A–defined minimally deleted regions had a mean decreased expression between 42% and 33%. In addition, 2 of these genes, *EZH2* and *RABL5*, were significantly down-regulated even in samples that did not have monosomy 7/del(7q). This current study showed that down-regulation of EZH2 in the absence of LOH is common in advanced MDS. These results point to the importance of haploinsufficiency of the genes located in the 7q CDRs in the pathobiology of MDS and suggests that other genetic or epigenetic mechanisms may silence these genes in cases without 7q LOH.

In summary, the present study of 7q disorders, gathering data from a large series of patients using recent genomics technologies, shows that SNP-A complements traditional MC not only by detection of cryptic abnormalities but also by precisely defining the extent and nature of the lesions with strong clinical associations. Although a 2-hit model is supported for most patients with UPD(7q) and a overlapping MDS/MPN phenotype, our results suggest that haploinsufficient expression of select regions of 7q is the driving pathogenetic mechanism in those patients with predominant dysplastic features and loss of chromosome 7 material.

Acknowledgments

This work was supported in part by National Institutes of Health grants R01 HL082983 (J.P.M.), U54 RR019391 (J.P.M., M.A.S.), and K24 HL077522 (J.P.M.); Department of Defense grant MPO48018 (M.A.M.); funds from Leukaemia & Lymphoma Research of the United Kingdom (A.P. and J.B.) and Fundacion Caja Madrid (A.J.); and a charitable donation from Robert Duggan Cancer Research Foundation.

The results published here were partly based on data generated by The Cancer Genome Atlas pilot project established by the National Cancer Institute and National Human Genome Research Institute. Information about TCGA and the investigators and institutions that constitute the TCGA research network can be found at http://cancergenome.nih.gov.

Authorship

Contribution: A.J., Y.S., and J.P.M. were responsible for overall design, data collection, analysis, and interpretation, statistical analysis, manuscript preparation, and writing and completion of the manuscript; H.M., A.V., A.M.J., B.P., V.V., R.V.T., C.L.O., A.M.M., and A.P. analyzed data and edited the manuscript; A.G.K., K.M., H.M., A.R.M., M.A.S., M.A.M., S.K., A.L., J.B., and G.J.M. gathered data and edited the manuscript; and all authors approved the final version of the manuscript and its submission.

Conflict-of-interest disclosure: The authors declare no competing financial interests.

Correspondence: Jaroslaw P. Maciejewski, Taussig Cancer Institution/R40, 9500 Euclid Ave, Cleveland, OH; e-mail: maciejj@ccf.org.

References

1. Slovak ML, Kopecky KJ, Cassileth PA, et al. Karyotypic analysis predicts outcome of preremission and postremission therapy in adult acute myeloid leukemia: a Southwest Oncology Group/Eastern Cooperative Oncology Group Study. *Blood*. 2000;96(13):4075-4083.
2. Hasle H, Arico M, Basso G, et al. Myelodysplastic syndrome, juvenile myelomonocytic leukemia, and acute myeloid leukemia associated with complete or partial monosomy 7. European Working Group on MDS in Childhood (EWOG-MDS). *Leukemia*. 1999;13(3):376-385.
3. Greenberg P, Cox C, LeBeau MM, et al. International scoring system for evaluating prognosis in myelodysplastic syndromes. *Blood*. 1997;89(6):2079-2088.
4. Grimwade D, Hills RK, Moorman AV, et al. Refinement of cytogenetic classification in acute myeloid leukemia: determination of prognostic significance of rare recurring chromosomal abnormalities among 5876 younger adult patients treated in the United Kingdom Medical Research Council trials. *Blood*. 2010;116(3):354-365.
5. Swansbury GJ, Lawler SD, Alimena G, et al. Long-term survival in acute myelogenous leukemia: a second follow-up of the Fourth International Workshop on Chromosomes in Leukemia. *Cancer Genet Cytogenet*. 1994;73(1):1-7.
6. Cordoba I, Gonzalez-Porras JR, Nomdedeu B, et al. Better prognosis for patients with del(7q) than for patients with monosomy 7 in myelodysplastic syndrome. *Cancer*. 2012;118(1):127-133.
7. Lai JL, Preudhomme C, Zandecki M, et al. Myelodysplastic syndromes and acute myeloid leukemia with 17p deletion. An entity characterized by specific dysgranulopoiesis and a high incidence of P53 mutations. *Leukemia*. 1995;9(3):370-381.
8. Fidler C, Watkins F, Bowen DT, Littlewood TJ, Wainscoat JS, Boultwood J. NRAS, FLT3 and TP53 mutations in patients with myelodysplastic syndrome and a del(5q). *Haematologica*. 2004;89(7):865-866.
9. Dunbar AJ, Gondek LP, O'Keefe CL, et al. 250K single nucleotide polymorphism array karyotyping identifies acquired uniparental disomy and homozygous mutations, including novel missense substitutions of c-Cbl, in myeloid malignancies. *Cancer Res*. 2008;68(24):10349-10357.
10. Delhommeau F, Dupont S, Della Valle V, et al. Mutation in TET2 in myeloid cancers. *N Engl J Med*. 2009;360(22):2289-2301.
11. Fero ML, Randel E, Gurley KE, Roberts JM, Kemp CJ. The murine gene p27Kip1 is haploinsufficient for tumour suppression. *Nature*. 1998;396(6707):177-180.
12. Venkatachalam S, Tyner SD, Pickering CR, et al. Is p53 haploinsufficient for tumor suppression? Implications for the p53+/– mouse model in carcinogenicity testing. *Toxicol Pathol*. 2001;29 Suppl:147-154.
13. Ebert BL, Pretz J, Bosco J, et al. Identification of RPS14 as a 5q- syndrome gene by RNA interference screen. *Nature*. 2008;451(7176):335-339.
14. Stein BL, Williams DM, O'Keefe C, et al. Disruption of the ASXL1 gene is frequent in primary, post-essential thrombocytosis and post-polycythemia vera myelofibrosis, but not essential thrombocytosis or polycythemia vera: analysis of molecular genetics and clinical phenotypes. *Haematologica*. 2011;96(10):1462-1469.
15. Pellagatti A, Cazzola M, Giagounidis A, et al. Marked down-regulation of nucleophosmin-1 is associated with advanced del(5q) myelodysplastic syndrome. *Br J Haematol*. 2011;155(2):272-274.
16. Pellagatti A, Cazzola M, Giagounidis A, et al. Deregulated gene expression pathways in myelodysplastic syndrome hematopoietic stem cells. *Leukemia*. 2010;24(4):756-764.
17. Shaffer LG, Slovak ML, Campbell LJ, International Standing Committee on Human Cytogenetic Nomenclature. *ISCN 2009: An International System for Human Cytogenetic Nomenclature* (2009). Shaffer LG, Slovak ML, Campbell LJ, International Standing Committee on Human Cytogenetic Nomenclature, eds. Basel; Unionville, CT: Karger; 2009.
18. Tiu RV, Gondek LP, O'Keefe CL, et al. New lesions detected by single nucleotide polymorphism array-based chromosomal analysis have important clinical impact in acute myeloid leukemia. *J Clin Oncol*. 2009;27(31):5219-5226.
19. Onida F, Kantarjian HM, Smith TL, et al. Prognostic factors and scoring systems in chronic myelomonocytic leukemia: a retrospective analysis of 213 patients. *Blood*. 2002;99(3):840-849.
20. Makishima H, Jankowska AM, Tiu RV, et al. Novel homo- and hemizygous mutations in EZH2 in myeloid malignancies. *Leukemia*. 2010;24(10):1799-1804.
21. Ernst T, Chase AJ, Score J, et al. Inactivating mutations of the histone methyltransferase gene EZH2 in myeloid disorders. *Nat Genet*. 2010;42(8):722-726.
22. Middeldorp A, van Puijenbroek M, Nielsen M, et al. High frequency of copy-neutral LOH in MUTYH-associated polyposis carcinomas. *J Pathol*. 2008;216(1):25-31.
23. Such E, Cervera J, Costa D, et al. Cytogenetic risk stratification in chronic myelomonocytic leukemia. *Haematologica*. 2011;96(3):375-383.
24. Young NS, Calado RT, Scheinberg P. Current concepts in the pathophysiology and treatment of aplastic anemia. *Blood*. 2006;108(8):2509-2519.
25. Yue G, Hao S, Fadare O, et al. Hypocellularity in myelodysplastic syndrome is an independent factor which predicts a favorable outcome. *Leuk Res*. 2008;32(4):553-558.
26. Huang TC, Ko BS, Tang JL, et al. Comparison of hypoplastic myelodysplastic syndrome (MDS) with normo-/hypercellular MDS by International Prognostic Scoring System, cytogenetic and genetic studies. *Leukemia*. 2008;22(3):544-550.
27. Jerez A, Gondek LP, Jankowska AM, et al. Topography, clinical, and genomic correlates of 5q myeloid malignancies revisited. *J Clin Oncol*. 2012;30(12):1343-1349.
28. Galván AB, Mallo M, Arenillas L, et al. Does monosomy 5 really exist in myelodysplastic syndromes and acute myeloid leukemia? *Leuk Res*. 2010;34(9):1242-1245.
29. Nilsson L, Astrand-Grundstrom I, Arvidsson I, et al. Isolation and characterization of hematopoietic progenitor/stem cells in 5q-deleted myelodysplastic syndromes: evidence for involvement at the hematopoietic stem cell level. *Blood*. 2000;96(6):2012-2021.
30. Nilsson L, Eden P, Olsson E, et al. The molecular signature of MDS stem cells supports a stem-cell origin of 5q myelodysplastic syndromes. *Blood*. 2007;110(8):3005-3014.
31. Le Beau MM, Espinosa R 3rd, et al. Cytogenetic and molecular delineation of a region of chromosome 7 commonly deleted in malignant myeloid diseases. *Blood*. 1996;88(6):1930-1935.
32. Döhner K, Brown J, Hehmann U, et al. Molecular cytogenetic characterization of a critical region in bands 7q35-q36 commonly deleted in malignant myeloid disorders. *Blood*. 1998;92(11):4031-4035.

Brief report

Somatic mosaicism for oncogenic *NRAS* mutations in juvenile myelomonocytic leukemia

Sayoko Doisaki,[1] Hideki Muramatsu,[1] Akira Shimada,[1] Yoshiyuki Takahashi,[1] Makiko Mori-Ezaki,[2] Masanori Sato,[3] Hiroyuki Kawaguchi,[4] Akitoshi Kinoshita,[5] Manabu Sotomatsu,[6] Yasuhide Hayashi,[6] Yoko Furukawa-Hibi,[7] Kiyofumi Yamada,[7] Hideaki Hoshino,[8] Hitoshi Kiyoi,[8] Nao Yoshida,[9] Hirotoshi Sakaguchi,[1] Atsushi Narita,[1] Xinan Wang,[1] Olfat Ismael,[1] Yinyan Xu,[1] Nobuhiro Nishio,[1] Makito Tanaka,[1] Asahito Hama,[1] Kenichi Koike,[10] and Seiji Kojima[1]

[1]Department of Pediatrics, Nagoya University Graduate School of Medicine, Nagoya, Japan; [2]Department of Hematology Oncology, Saitama Children's Medical Center, Saitama, Japan; [3]Department of Pediatrics, Tokyo Dental College Ichikawa General Hospital, Ichikawa, Japan; [4]Department of Pediatrics, National Defense Medical College, Tokorozawa, Japan; [5]Department of Pediatrics, St Marianna University School of Medicine, Kawasaki, Japan; [6]Department of Hematology/Oncology, Gunma Children's Medical Center, Shibukawa, Japan; [7]Department of Neuropsychopharmacology and Hospital Pharmacy, Nagoya University Graduate School of Medicine, Nagoya, Japan; [8]Department of Hematology and Oncology, Nagoya University Graduate School of Medicine, Nagoya, Japan; [9]Department of Pediatrics, Japanese Red Cross Nagoya First Hospital, Nagoya, Japan; and [10]Department of Pediatrics, Shinshu University School of Medicine, Matsumoto, Japan

Juvenile myelomonocytic leukemia (JMML) is a rare pediatric myeloid neoplasm characterized by excessive proliferation of myelomonocytic cells. Somatic mutations in genes involved in GM-CSF signal transduction, such as *NRAS*, *KRAS*, *PTPN11*, *NF1*, and *CBL*, have been identified in more than 70% of children with JMML. In the present study, we report 2 patients with somatic mosaicism for oncogenic *NRAS* mutations (G12D and G12S) associated with the development of JMML. The mutated allele frequencies quantified by pyrosequencing were various and ranged from 3%-50% in BM and other somatic cells (ie, buccal smear cells, hair bulbs, or nails). Both patients experienced spontaneous improvement of clinical symptoms and leukocytosis due to JMML without hematopoietic stem cell transplantation. These patients are the first reported to have somatic mosaicism for oncogenic *NRAS* mutations. The clinical course of these patients suggests that *NRAS* mosaicism may be associated with a mild disease phenotype in JMML. (*Blood*. 2012;120(7):1485-1488)

Introduction

Juvenile myelomonocytic leukemia (JMML) is a rare myeloid neoplasm characterized by excessive proliferation of myelomonocytic cells. Somatic mutations in genes involved in GM-CSF signal transduction, such as *NRAS*, *KRAS*, *PTPN11*, *NF1*, and *CBL*, have been identified in more than 70% of children with JMML.[1-3] The term "somatic mosaicism" is defined as the presence of multiple populations of cells with distinct genotypes in one person whose developmental lineages trace back to a single fertilized egg.[4] Somatic mosaicism of various genes, including some oncogenes, has been implicated in many diseases. For example, somatic mosaicism for *HRAS* mutations is found in patients with Costello syndrome.[5-7] Whereas germline mutations in causative genes (ie, *PTPN11*, *NRAS*, *NF1*, and *CBL*) are found in JMML patients,[3,8-11] the presence of somatic mosaicism for these genes has never been reported. In the present study, we describe 2 cases of JMML in which the patients display somatic mosaicism for oncogenic *NRAS* mutations (G12D and G12S).

Study design

Written informed consent for sample collection was obtained from the patients' parents in accordance with the Declaration of Helsinki, and molecular analysis of the mutational status was approved by the ethics committee of the Nagoya University Graduate School of Medicine (Nagoya, Japan).

Patient 1. A 10-month-old boy had hepatosplenomegaly and leukocytosis (72.1×10^9/L) with monocytosis (13.3×10^9/L; Table 1). The patient's BM contained 7% blasts with myeloid hyperplasia. Cytogenetic analysis revealed a normal karyotype and colony assay of BM mononuclear cells (BM-MNCs) showed spontaneous colony formation but GM-CSF hypersensitivity assay was not tested. The diagnostic criteria for JMML, as developed by the European Working Group on Myelodysplastic Syndrome in Childhood, was fulfilled,[12] and the patient was treated with IFN-α and 6-mercaptopurine. His clinical and laboratory findings gradually resolved without hematopoietic stem cell transplantation. However, 11 years after the diagnosis of JMML, the patient developed thrombocytopenia (7.6×10^9/L) and BM findings showed trilineage dysplasia with low blast count compatible with refractory anemia. The patient did not have any physiologic abnormalities, such as facial deformity, and there was no family history of malignancy or congenital abnormalities.

Patient 2. A 10-month-old boy had anemia, hepatosplenomegaly, and leukocytosis (31.8×10^9/L) with monocytosis (6.4×10^9/L; Table 1). The patient's BM exhibited myeloid hyperplasia and granulocytic dysplasia with 5% blasts. Cytogenetic

Submitted February 3, 2012; accepted June 11, 2012. Prepublished online as *Blood* First Edition paper, July 2, 2012; DOI 10.1182/blood-2012-02-406090.

The online version of this article contains a data supplement.

The publication costs of this article were defrayed in part by page charge payment. Therefore, and solely to indicate this fact, this article is hereby marked "advertisement" in accordance with 18 USC section 1734.

Table 1. Patient characteristics

	Patient 1	Patient 2
Age, mo	10	10
Sex	Male	Male
Liver, cm	12	5
Spleen, cm	8	10
WBCs, $\times 10^9$/L	72.1	31.8
Monocytes, %	18.5	20
Blasts, %	4	2
Hb, g/dL	8.9	5.4
Platelets, $\times 10^9$/L	59	100
HbF, %	2.1	1.7
BM blasts, %	7	5
Karyotype	46,XY [20/20]	46,XY [20/20]
Monosomy 7 (FISH)	Negative	Negative
Spontaneous colony formation	Positive	Positive
Gene mutation	*NRAS*, G12D 35G > A	*NRAS*, G12S 34G > A
Treatment	IFN-α-2b, 6-MP	None
Observation period, mo	231	103
Outcome	Alive	Alive
Fraction of mutant alleles, % (pyrosequencing)		
Nail (whole)	24	12.5 (average)
Nail (left hand)	ND	26
Nail (right hand)	ND	13
Nail (left foot)	ND	8
Nail (right foot)	ND	3
Buccal smear cells	43	21
Hair bulbs	5	ND
Family studies		
Father	Wild-type	Wild-type
Mother	Wild-type	Wild-type
Sibling	ND	Wild-type

Hb indicates hemoglobin; 6-MP, 6-mercaptopurine; and ND, not done.

analysis revealed a normal karyotype. Colony assay of BM-MNCs showed spontaneous colony formation and GM-CSF hypersensitivity. Although the diagnostic criteria for JMML were fulfilled,[12] the patient's clinical symptoms and leukocytosis improved spontaneously within a few months without cytotoxic therapy or hematopoietic stem cell transplantation. The patient has remained healthy and has experienced no hematologic or physiologic abnormalities. The most recent follow-up examination was conducted when the patient was 8 years of age.

Detailed methods for experiments are described in supplemental Methods (available on the *Blood* Web site; see the Supplemental Materials link at the top of the online article).

Results and discussion

DNA sequencing for JMML-associated genes (ie, *NRAS*, *KRAS*, *PTPN11*, and *CBL*) was performed (Figure 1 and Table 1). In Patient 1, the *NRAS* G12D mutation was identified in BM-MNCs at the time of diagnosis of both JMML and MDS. We identified the same G12D mutation in DNA derived from buccal smear cells and nails of both hands; however, the sequence profile of the nails showed a low signal for the mutant allele compared with signal of blood cells. In Patient 2, the *NRAS* G12S mutation was identified in DNA from BM-MNCs, buccal smear cells, and nails of the left hand. However, the sequence profiles of buccal smear cells and nails of the left hand showed a low signal for the mutant variant. No mutation was detected in DNA from the PB-MNCs of the patient's parents or sibling.

We used pyrosequencing to quantify the fraction of mutated alleles in DNA samples from different somatic tissues (Figure 1 and Table 1). The frequency of mutated alleles varied by tissue type as follows. For Patient 1: BM-MNCs, 50%; nails, 24%; buccal smear cells, 43%; and hair bulbs, 5%. For Patient 2: buccal smear cells, 21%; nails of left hand, 26%; nails of right hand, 13%; nails of left foot, 8%; and nails of right foot, 3%. We cloned the PCR product of *NRAS* exon 2 from the nails of Patient 1 and picked up 15 clones. The clones were sequenced. Four of the 15 clones (27%) contained the mutant allele, which is consistent with the results of pyrosequencing analysis (24% mutant allele). Because the confirmed detection level by pyrosequencing technique was above 5%, results with a low percentage (< 5%) of mutant allele (ie, hair bulbs in Patient 1) should be interpreted with caution.[13,14]

We diagnosed 2 JMML patients as having somatic mosaicism of *NRAS* mutations: G12D for Patient 1 and G12S for Patient 2. The diagnoses were based on negative familial studies and mutational allele quantification analyses that showed diversity in the chimeric mutational status of different somatic tissues. Although DNA from buccal smear cells might be contaminated with WBCs, we also identified mutations in DNA from the nail tissue, which is known to be a good biologic material without contamination from hematopoietic cells, in both patients. These data suggest that a portion of the *NRAS*-mutated somatic cells were derived from one cell that acquired the mutation at a very early developmental stage. Although both somatic and germline mutations of RAS pathway genes (ie, *PTPN11*, *NRAS*, *NF1*, and *CBL*) are found in some JMML patients,[3,8-11] somatic mosaicism for these genes has never been reported. To the best of our knowledge, the present study is

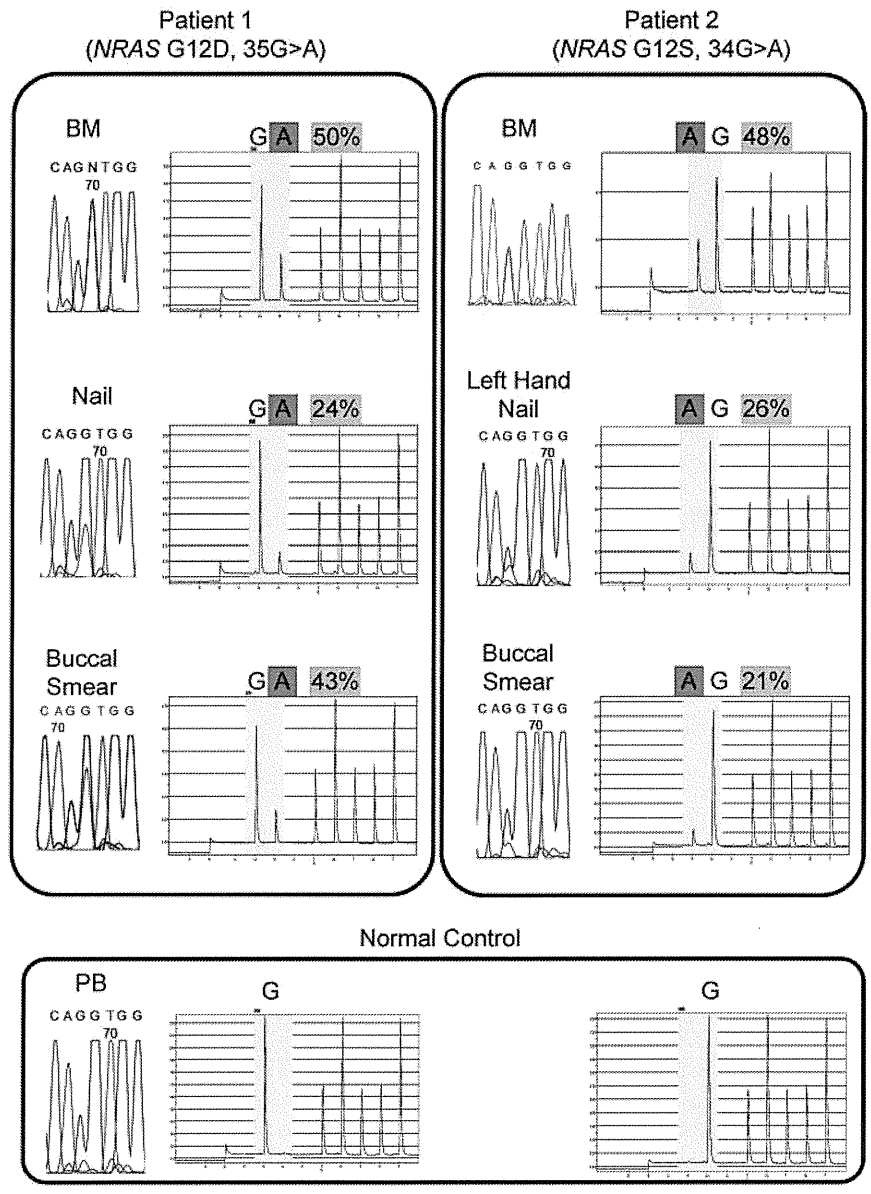

Figure 1. Direct sequencing and quantitative mutational analysis of *NRAS* in JMML patients. *NRAS* mutations are detected by direct sequencing and quantified by pyrosequencing. Direct sequencing identified oncogenic *NRAS* mutations: for Patient 1, G12D, 35G > A; for Patient 2, G12S, 34G > A) in BM-MNCs at diagnosis of JMML and in the nails and buccal smear cells. Quantification by pyrosequencing revealed that the fractions of mutated allele varied among different tissue types. For Patient 1: BM, 50%; nail, 24%; and buccal smear, 43%. For Patient 2: BM, 48%; left-hand nail, 26%; and buccal smear, 21%.

the first report of JMML patients with somatic mosaicism of mutations in RAS pathway genes.

Germline RAS pathway mutations are often associated with dysmorphic features similar to Noonan syndrome or its associated diseases. Correspondingly, JMML patients with germline *NRAS* or *CBL* mutations exhibit characteristic dysmorphic features.[3,10] Although our patients did not show any dysmorphic or developmental abnormalities, they should receive careful medical follow-up, especially for the occurrence of other cancers, because of the oncogenic nature of the mutations.

In general, JMML is a rapidly fatal disorder if left untreated.[8] However, recent clinical genotype-phenotype analyses have revealed heterogeneity in their clinical course. We and other researchers have reported that patients with *PTPN11* mutations have a worse prognosis than patients with other gene mutations, including *NRAS* and *KRAS*.[15,16] Both of the JMML patients in the present study with somatic mosaicism of oncogenic *NRAS* mutations have had a mild and self-limiting clinical course. We analyzed nails of other 3 JMML patients with RAS mutations who experienced aggressive clinical course and none showed somatic mosaicism (data not shown). In analogy to the mild phenotype of JMML patients with germline mutations in *PTPN11*, we speculate that JMML patients with somatic mosaicism of RAS genes might have a mild clinical course. We are planning to confirm these observations in larger cohort.

Acknowledgments

The authors thank Ms Yoshie Miura, Ms Yuko Imanishi, and Ms Hiroe Namizaki for their valuable assistance with sample preparation and clerical work.

Authorship

Contribution: S.D. and H.M. designed and conducted the research, analyzed the data, and wrote the manuscript; A.S., M.M.-E., M. Sato, H.K., A.K., M. Sotomatsu, and Y.H. treated the patients; Y.T., Y.F.-H., K.Y., H.H., H.K., N.Y., H.S., A.N., X.W., O.I., Y.X.,

N.N., M.T., A.H., and K.K. conducted the research; and S.K. designed the research, analyzed the data, and wrote the manuscript.

Conflict-of-interest disclosure: The authors declare no competing financial interests.

Correspondence: Seiji Kojima, Department of Pediatrics, Nagoya University Graduate School of Medicine, 65 Tsuruma-cho, Showa-ku, Nagoya 466-8550, Japan; e-mail: kojimas@med.nagoya-u.ac.jp.

References

1. Flotho C, Kratz CP, Niemeyer CM. How a rare pediatric neoplasia can give important insights into biological concepts: a perspective on juvenile myelomonocytic leukemia. *Haematologica.* 2007; 92(11):1441-1446.
2. Muramatsu H, Makishima H, Jankowska AM, et al. Mutations of an E3 ubiquitin ligase c-Cbl but not TET2 mutations are pathogenic in juvenile myelomonocytic leukemia. *Blood.* 2010;115(10): 1969-1975.
3. Niemeyer CM, Kang MW, Shin DH, et al. Germline CBL mutations cause developmental abnormalities and predispose to juvenile myelomonocytic leukemia. *Nat Genet.* 2010;42(9):794-800.
4. Cotterman CW. Somatic mosaicism for antigen A2. *Acta Genet Stat Med.* 1956;6(4):520-521.
5. Gripp KW, Stabley DL, Nicholson L, Hoffman JD, Sol-Church K. Somatic mosaicism for an HRAS mutation causes Costello syndrome. *Am J Med Genet A.* 2006;140(20):2163-2169.
6. Sol-Church K, Stabley DL, Demmer LA, et al. Male-to-male transmission of Costello syndrome: G12S HRAS germline mutation inherited from a father with somatic mosaicism. *Am J Med Genet A.* 2009;149A(3):315-321.
7. Girisha KM, Lewis LE, Phadke SR, Kutsche K. Costello syndrome with severe cutis laxa and mosaic HRAS G12S mutation. *Am J Med Genet A.* 2010;152A(11):2861-2864.
8. Niemeyer CM, Arico M, Basso G, et al. Chronic myelomonocytic leukemia in childhood: a retrospective analysis of 110 cases. European Working Group on Myelodysplastic Syndromes in Childhood (EWOG-MDS). *Blood.* 1997;89(10): 3534-3543.
9. Tartaglia M, Niemeyer CM, Fragale A, et al. Somatic mutations in PTPN11 in juvenile myelomonocytic leukemia, myelodysplastic syndromes and acute myeloid leukemia. *Nat Genet.* 2003; 34(2):148-150.
10. De Filippi P, Zecca M, Lisini D, et al. Germ-line mutation of the NRAS gene may be responsible for the development of juvenile myelomonocytic leukaemia. *Br J Haematol.* 2009;147(5):706-709.
11. Side LE, Emanuel PD, Taylor B, et al. Mutations of the NF1 gene in children with juvenile myelomonocytic leukemia without clinical evidence of neurofibromatosis, type 1. *Blood.* 1998;92(1): 267-272.
12. Pinkel D. Differentiating juvenile myelomonocytic leukemia from infectious disease [letter]. *Blood.* 1998;91(1):365-367.
13. Fakhrai-Rad H, Pourmand N, Ronaghi M. Pyrosequencing: an accurate detection platform for single nucleotide polymorphisms. *Hum Mutat.* 2002;19(5):479-485.
14. Ogino S, Kawasaki T, Brahmandam M, et al. Sensitive sequencing method for KRAS mutation detection by Pyrosequencing. *J Mol Diagn.* 2005; 7(3):413-421.
15. Bresolin S, Zecca M, Flotho C, et al. Gene expression-based classification as an independent predictor of clinical outcome in juvenile myelomonocytic leukemia. *J Clin Oncol.* 2010; 28(11):1919-1927.
16. Yoshida N, Yagasaki H, Xu Y, et al. Correlation of clinical features with the mutational status of GM-CSF signaling pathway-related genes in juvenile myelomonocytic leukemia. *Pediatr Res.* 2009;65(3):334-340.

The EMBO Journal (2012) 00, 1–13 | © 2012 European Molecular Biology Organization | All Rights Reserved 0261-4189/12
www.embojournal.org

THE EMBO JOURNAL

Histone chaperone activity of Fanconi anemia proteins, FANCD2 and FANCI, is required for DNA crosslink repair

Koichi Sato[1,7], Masamichi Ishiai[2,7], Kazue Toda[1], Satoshi Furukoshi[1], Akihisa Osakabe[1], Hiroaki Tachiwana[1], Yoshimasa Takizawa[1], Wataru Kagawa[1], Hiroyuki Kitao[2,3], Naoshi Dohmae[4], Chikashi Obuse[5], Hiroshi Kimura[6], Minoru Takata[2,*] and Hitoshi Kurumizaka[1,*]

[1]Laboratory of Structural Biology, Graduate School of Advanced Science and Engineering, Waseda University, Tokyo, Japan, [2]Laboratory of DNA Damage Signaling, Department of Late Effects Studies, Radiation Biology Center, Kyoto University, Kyoto, Japan, [3]Graduate School of Medical Sciences, Department of Molecular Oncology, Kyushu University, Fukuoka, Japan, [4]RIKEN Advanced Science Institute, Saitama, Japan, [5]Graduate School of Life Science, Hokkaido University, Hokkaido, Japan and [6]Graduate School of Frontier Biosciences, Osaka University, Osaka, Japan

Fanconi anaemia (FA) is a rare hereditary disorder characterized by genomic instability and cancer susceptibility. A key FA protein, FANCD2, is targeted to chromatin with its partner, FANCI, and plays a critical role in DNA crosslink repair. However, the molecular function of chromatin-bound FANCD2-FANCI is still poorly understood. In the present study, we found that FANCD2 possesses nucleosome-assembly activity *in vitro*. The mobility of histone H3 was reduced in FANCD2-knockdown cells following treatment with an interstrand DNA crosslinker, mitomycin C. Furthermore, cells harbouring FANCD2 mutations that were defective in nucleosome assembly displayed impaired survival upon cisplatin treatment. Although FANCI by itself lacked nucleosome-assembly activity, it significantly stimulated FANCD2-mediated nucleosome assembly. These observations suggest that FANCD2-FANCI may regulate chromatin dynamics during DNA repair.

The EMBO Journal advance online publication, 24 July 2012; doi:10.1038/emboj.2012.197

Subject Categories: genome stability & dynamics; chromatin & transcription

Keywords: DNA repair; FANCD2; FANCI; Fanconi anaemia; histone chaperone

*Corresponding authors. M Takata, Laboratory of DNA Damage Signaling, Radiation Biology Center, Kyoto University, Yoshida-konoe, Sakyo-ku, Kyoto 606-8501, Japan. Tel.: +81 75 753 7563; Fax: +81 75 753 7565; E-mail: mtakata@house.rbc.kyoto-u.ac.jp or H Kurumizaka, Laboratory of Structural Biology, Graduate School of Advanced Science and Engineering, Waseda University, 2-2 Wakamatsu-cho, Shinjuku-ku, Tokyo 162-8480, Japan. Tel.: +81 3 5369 7315; Fax: +81 3 5367 2820; E-mail: kurumizaka@waseda.jp
[7]These authors contributed equally to this work

Received: 17 June 2012; accepted: 3 July 2012

Introduction

Fanconi anaemia (FA) is a rare hereditary disorder characterized by skeletal abnormalities, progressive bone marrow failure, and genomic instability accompanied by cancer susceptibility (Venkitaraman, 2004; Niedernhofer *et al*, 2005; Taniguchi and D'Andrea, 2006; Wang, 2007). FA-mutant cells are highly sensitive to interstrand DNA crosslinking reagents, which induce stalled replication forks, suggesting that FA proteins promote the stabilization and restarting of the replisome (Thompson *et al*, 2005; Wang, 2007).

Thirteen genes, *FANCA*, *-B*, *-C*, *-D1* (*BRCA2*), *-D2*, *-E*, *-F*, *-G*, *-I*, *-J* (*BRIP1*), *-L*, *-M*, and *-N* (*PALB2*), corresponding to individual FA complementation groups, have been cloned (Thompson *et al*, 2005; Wang, 2007; Kee and D'Andrea, 2010; Garner and Smogorzewska, 2011; Kitao and Takata, 2011). In addition, homozygous Rad51C mutations have recently been identified in a family with an FA-like disorder, as the *FANCO* gene (Vaz *et al*, 2010), and *SLX4* has been confirmed as the *FANCP* gene (Crossan *et al*, 2011; Kim *et al*, 2011; Stoepker *et al*, 2011). These FA gene products constitute a common DNA damage response pathway that is often referred to as the 'FA pathway'. In this pathway, eight proteins, FANCA, -B, -C, -E, -F, -G, -L, and -M, and three FANCA-associated polypeptides (FAAPs) form the FA core E3 ligase complex (Garcia-Higuera *et al*, 2001; Wang, 2007; Ali *et al*, 2012; Kim *et al*, 2012; Leung *et al*, 2012). On the other hand, FANCD2 and FANCI associate with each other to form a different complex, called the ID complex (Sims *et al*, 2007; Smogorzewska *et al*, 2007).

Upon DNA damage during S-phase, multiple phosphorylations of FANCI trigger the monoubiquitination of FANCD2 and FANCI by the FA core complex (Ishiai *et al*, 2008). The monoubiquitinated ID complex is then targeted to the chromatin, where it plays a critical role in DNA-repair pathways, such as homologous recombination and translesion synthesis (Matsushita *et al*, 2005; Thompson *et al*, 2005; Yamamoto *et al*, 2005; Wang, 2007; Kee and D'Andrea, 2010; Garner and Smogorzewska, 2011; Kitao and Takata, 2011). Recent studies indicated that monoubiquitinated FANCD2 (and FANCI) recruit the FAN1 nuclease, which possesses endo- and exonuclease activities, providing a partial explanation for their roles in DNA repair (Kratz *et al*, 2010; MacKay *et al*, 2010; Smogorzewska *et al*, 2010; Yoshikiyo *et al*, 2010). Monoubiquitinated FANCD2 also reportedly recruits SLX4 (Garner and Smogorzewska, 2011; Yamamoto *et al*, 2011), which is considered to function as a scaffold that interacts with the other nucleases, SLX1, XPF, and MUS81 (Fekairi *et al*, 2009; Svendsen *et al*, 2009; Yamamoto *et al*, 2011). Furthermore, a recent report found that FANCD2 itself might have exonuclease activity (Pace *et al*, 2010). However, whether chromatin-bound FANCD2 and FANCI have any additional functions remains to be determined.

The nucleosome is the fundamental repeating unit of chromatin (Wolffe, 1998). Four core histones, H2A, H2B,

H3, and H4, are the protein components of the nucleosome. H2A forms a specific dimer with H2B (H2A/H2B dimer), and H3 forms a specific dimer with H4 (H3/H4 dimer). During nucleosome assembly, two H3/H4 dimers (H3/H4 tetramer) are first deposited on DNA, forming a tetrasome, in which the DNA is wrapped around the H3/H4 tetramer. Two H2A/H2B dimers are then incorporated into the tetrasome to form the mature nucleosome, in which about 150 base pairs of DNA are wrapped around a histone octamer, containing two each of the H2A/H2B and H3/H4 dimers. In cells, nucleosomes are dynamically assembled and disassembled during the replication, transcription, recombination, and repair processes, and such nucleosome dynamics are accomplished with the aid of histone chaperones and/or ATP-dependent chromatin remodelling factors (Avvakumov *et al*, 2011).

In the present study, we purified the human and chicken FANCD2 proteins, and found that FANCD2 possesses nucleosome-assembly activity *in vitro*. We also purified FANCI, and showed that it significantly stimulated FANCD2-mediated nucleosome assembly, although FANCI itself lacked nucleosome-assembly activity. A histone-binding domain was mapped in the chicken FANCD2 C-terminal region (residues 1268–1439). The FANCD2 mutants, in which either the histone-binding domain was deleted or the Arg1336 and Lys1346 residues were replaced by Ala, were significantly defective in nucleosome assembly *in vitro*, and cells bearing these mutants displayed impaired survival upon cisplatin treatment *in vivo*. Furthermore, a disease-related mutation, human FANCD2(R302W) (Timmers *et al*, 2001), compromised histone dynamics, and the corresponding chicken FANCD2(R305W) also showed impaired histone chaperone activity. These data suggest that the histone chaperone activity of FANCD2 is crucial for the histone dynamics and the DNA crosslink repair in cells.

Results

Human FANCD2 promotes nucleosome assembly

In a proteome analysis to search for proteins in HeLa cell extracts that bind to the histone H3/H4 complex (Supplementary Figure S1), we unexpectedly detected human FANCD2 (hFANCD2) as a candidate interacting protein. Indeed, hFANCD2 was efficiently captured from a HeLa cell extract, using H3/H4 beads (Figure 1A). We purified hFANCD2 as a recombinant protein expressed in insect cells (Supplementary Figure S2A), and confirmed that purified hFANCD2 also bound to H3/H4 (Figure 1B). The hFANCD2-H3/H4 binding was also detected in the presence of DNaseI (Figure 1B, lane 5), indicating that the interaction is not mediated by DNA contamination. These results indicated that hFANCD2 directly binds to H3/H4, which prompted us to examine its nucleosome-assembly activity.

We tested hFANCD2-mediated nucleosome assembly by a topological assay, using relaxed circular DNA in the presence of topoisomerase (Figure 1C). The extent of nucleosome formation was assessed by analysing the superhelicity of circular DNA fractionated through an agarose gel, because negative supercoils are introduced when nucleosomes are formed. As shown in Figure 1C, the number of superhelical turns in the DNA substrate increased with greater amounts of hFANCD2. The faster migration of the DNA substrate was not due to DNA degradation (Supplementary Figure S2B). Therefore, hFANCD2 actually promoted nucleosome assembly *in vitro*. We next performed the nucleosome-assembly assay with a short DNA fragment, to directly detect the nucleosomes by an electrophoretic mobility shift assay. hFANCD2 stimulated the nucleosome assembly in this assay (Figure 1D, lanes 6–9). The nucleosome-assembly activity of hFANCD2 was slightly lower than that of human Nap1, which is a prominent nucleosome-assembly protein (Figure 1D). These biochemical results suggest that FANCD2 may regulate chromatin reorganization during DNA repair in higher eukaryotes.

Chromatin-bound FANCD2 is known to be monoubiquitinated, and the ubiquitin moiety may function to recruit its associated nucleases (Fekairi *et al*, 2009; Svendsen *et al*, 2009; Kratz *et al*, 2010; MacKay *et al*, 2010; Smogorzewska *et al*, 2010; Yoshikiyo *et al*, 2010; Yamamoto *et al*, 2011). Therefore, we tested whether FANCD2 monoubiquitination affects the nucleosome-assembly activity. For this purpose, we utilized the chicken FANCD2 protein (cFANCD2) (Yamamoto *et al*, 2005), which was bacterially expressed and purified to homogeneity (Supplementary Figure S2C). We then prepared monoubiquitinated cFANCD2, using purified components for the conjugation (i.e., FANCL, UBE2T, E1, and ubiquitin; Supplementary Figure S2D–F). As we previously reported, the cFANCD2 monoubiquitination was robustly enhanced in the presence of DNA (Sato *et al*, 2012), and about 40% of cFANCD2 was monoubiquitinated in this study (Supplementary Figure S2F). This monoubiquitinated cFANCD2 fraction was purified, and was subjected to the topological assay. However, we did not find a clear difference in the nucleosome-assembly activities between the fractions containing monoubiquitinated cFANCD2 and the monoubiquitination-deficient cFANCD2(K563R) mutant (Supplementary Figure S2G). Therefore, the monoubiquitination does not affect the activity. However, this could be due to the incomplete monoubiquitination of cFANCD2. Therefore, we prepared the monoubiquitination-mimicking version of FANCD2, by genetically fusing FANCD2(K563R) with ubiquitin to create FANCD2(K563R)-Ub (Supplementary Figure S2H), which is known to complement the DNA-repair-defective phenotype in the *FANCD2*$^{-/-}$ DT40 cells (Matsushita *et al*, 2005). We found that purified FANCD2(K563R)-Ub possessed similar histone-binding and nucleosome-assembly activities to those of cFANCD2 (Supplementary Figure S2I and J). These results suggested that the FANCD2 monoubiquitination may not be directly involved in the nucleosome assembly.

The C-terminal region of FANCD2 is responsible for interacting with histone H3/H4 and for promoting nucleosome assembly

To gain further insights into the molecular mechanism and the functional relevance of the nucleosome-assembly activity of FANCD2, we first searched for the FANCD2 region that interacts with the H3/H4 complex. We subjected cFANCD2 to limited proteolysis, and two fragments, cFANCD2(1-1167) and cFANCD2(1-1389), were identified (Figure 2A). These fragments lacked the acidic region, which is composed of the C-terminal 50 amino-acid residues of FANCD2. In addition, FANCD2(1268X), which also lacks the C-terminal region, is present in FA patients (FA Mutation Database, http://www.rockefeller.edu/fanconi/mutate/), suggesting the functional

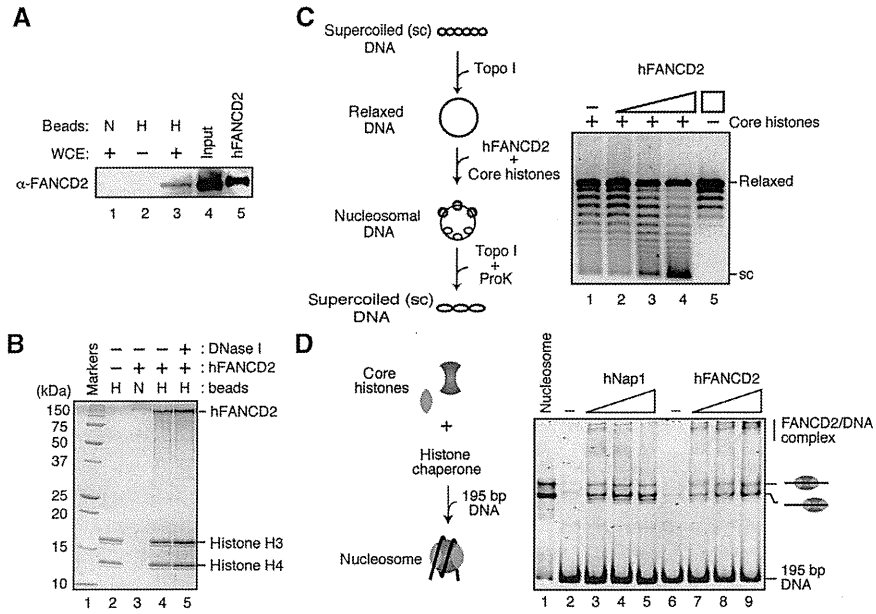

Figure 1 hFANCD2 promotes nucleosome assembly. (**A**) The H3/H4-conjugated beads were incubated with a HeLa WCE, and the endogenous FANCD2 bound to the beads was detected by western blotting with an anti-FANCD2 monoclonal antibody (α-FANCD2). N and H indicate the control Affi-Gel 10 beads and the H3/H4-conjugated beads, respectively. Input WCE (30 μg of protein) and hFANCD2 (125 ng) were applied in lanes 4 and 5, respectively. (**B**) The H3/H4 beads were incubated with purified hFANCD2 in the absence or presence of DNaseI, washed with buffer, and mixed with two-fold SDS sample buffer. The proteins bound to the beads were analysed by 15% SDS–PAGE. (**C**) Topological assay. A schematic diagram of topological assay is shown in the left panel. Nucleosomes were reconstituted on the relaxed plasmid DNA by hFANCD2 (0.2, 0.5, and 0.9 μM), in the presence of wheat germ topoisomerase I. After deproteinization, the topoisomers were separated by agarose gel electrophoresis. Highly supercoiled and relaxed DNAs are denoted as 'sc' and 'relaxed', respectively. (**D**) Nucleosome-assembly assay. A schematic diagram of the nucleosome-assembly assay is shown in the left panel. Nucleosomes were reconstituted on the linear 195 base-pair DNA by hNap1 (0.4, 0.8, and 1.6 μM) or hFANCD2 (0.2, 0.4, and 0.8 μM). Nucleosomes positioned at the edge and centre of the 195-bp DNA are indicated by cartoons on the right side of the panel.

importance of the FANCD2 C-terminal region. As histone chaperones are generally acidic, we investigated whether this acidic C-terminal region is essential for histone binding. The C-terminal deletion mutants, cFANCD2(1-1167), cFANCD2 (1-1267), and cFANCD2(1-1389), were expressed as GFP-tagged forms in HEK293T cells, and their H3/H4-binding activity was examined by a pull-down assay, using the H3/H4 beads. We found that cFANCD2(1-1167) and cFANCD2(1-1267) displayed diminished H3/H4 binding (Figure 2B, lanes 3 and 4). In contrast, cFANCD2(1-1389) retained residual H3/H4-binding activity (Figure 2B, lane 2). Consistently, cFANCD2(1-1167) and cFANCD2(1-1267) showed significant defects in nucleosome assembly (Figure 2C, lanes 13–17 and 18–22, and D; Supplementary Figure S3A). cFANCD2(1-1389) was completely proficient in the nucleosome-assembly activity under low protein concentration conditions (Figure 2C, lanes 8–12, and D; Supplementary Figure S3B). These observations suggest that the C-terminal region of FANCD2 (amino acids 1268–1389) is important for interacting with H3/H4 and for promoting nucleosome assembly. It should be noted that cFANCD2(1-1389) was defective in nucleosome assembly under high protein concentration conditions (Figure 2C, lanes 10–11, and D; Supplementary Figure S3C). This may reflect the biochemical property of cFANCD2(1-1389), which tends to form large protein–DNA aggregates that are unable to enter an agarose gel during electrophoresis (Supplementary Figure S3D).

Since the cFANCD2 C-terminal deletion may induce the improper folding of the cFANCD2 structure, we next performed the H3/H4-binding and nucleosome-assembly experiments with cFANCD2 point mutants. Based on the amino-acid conservation among the human, mouse, chicken, frog, fish, and fly FANCD2 proteins, we mutated the conserved amino-acid residues, which might be functionally important (Figure 2A). We found that the FANCD2(R1336A/K1346A) mutant, in which the Arg1336 and Lys1346 residues are replaced by Ala, was significantly defective in nucleosome assembly *in vitro*, while another mutant, cFANCD2(D1350A/E1365A/E1382A), in which the Asp1350, Glu1365, and Glu1382 residues are replaced by Ala, did not affect the nucleosome-assembly activity (Figure 2A, E, and F; Supplementary Figure S3E). Consistently, the histone-binding activity was substantially reduced in cFANCD2(R1336A/K1346A) (Figure 2B lane 11), but not in cFANCD2(D1350A/E1365A/E1382A) (Figure 2B, lane 10). These results strongly support the conclusion that FANCD2 promotes nucleosome assembly through its C-terminal histone-binding domain.

Finally, we tested the histone binding of the C-terminal cFANCD2 fragments, cFANCD2(669-1439) and cFANCD2 (953-1439), which contain the C-terminal amino-acid residues 669-1439 and 953-1439, respectively (Figure 2A). These cFANCD2 fragments were identified by a protease mapping experiment. As expected, the cFANCD2(669-1439) and cFANCD2(953-1439) fragments both efficiently bound to histones (Figure 2B, lanes 5 and 6). Surprisingly, cFANCD2 (953-1439), which contained only one-third of cFANCD2, promoted nucleosome assembly (Figure 2C, lanes 23–27, and D). Therefore, we concluded that the histone-binding domain is located in the C-terminal region of FANCD2.

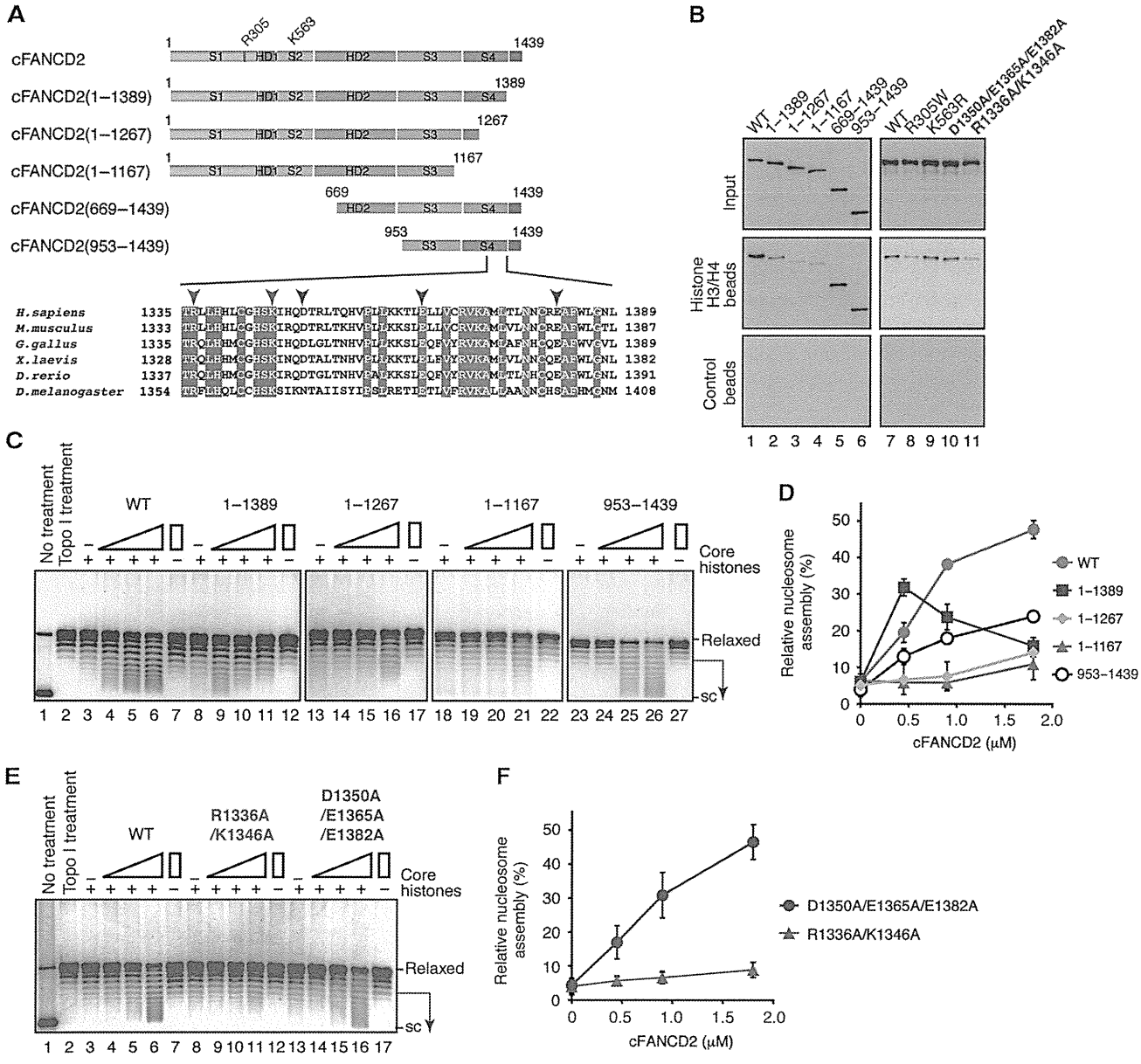

Figure 2 The C-terminal region of FANCD2 is responsible for histone binding and nucleosome assembly. (**A**) Schematic representations of full-length cFANCD2, and the cFANCD2(1-1389), cFANCD2(1-1267), cFANCD2(1-1167), cFANCD2(669-1439), and cFANCD2(953-1439) deletion mutants. The cFANCD2 domains, solenoid 1, helical domain 1, solenoid 2, helical domain 2, solenoid 3, and solenoid 4, are denoted as S1, HD1, S2, HD2, S3, and S4, respectively (Joo *et al*, 2011). The FANCD2 C-terminal acidic region is coloured red. The amino-acid sequences of the C-terminal regions of the *Homo sapiens*, *Mus musculus*, *Gallus gallus*, *Xenopus laevis*, *Danio rerio*, and *Drosophila melanogaster* FANCD2 proteins are aligned. The highly conserved residues are coloured red. The mutated residues in cFANCD2(R1336A/K1346A) and cFANCD2(D1350A/E1365A/E1382A) are indicated by orange and purple arrowheads, respectively. (**B**) The H3/H4 beads were incubated with extracts of HEK293T cells, producing either GFP-tagged cFANCD2, cFANCD2(1-1389), cFANCD2(1-1267), cFANCD2(1-1167), cFANCD2(669-1439), cFANCD2(953-1439), cFANCD2(R305W), cFANCD2(K563R), cFANCD2(D1350A/E1365A/E1382A), or cFANCD2 (R1336A/K1346A). Proteins bound to the beads were detected by western blotting with an anti-chFANCD2 (polyclonal) antibody. The bottom panel indicates negative control experiments with beads lacking histones. (**C**) Nucleosomes were reconstituted on the relaxed plasmid DNA by cFANCD2 (lanes 3–7), cFANCD2(1-1389) (lanes 8–12), cFANCD2(1-1267) (lanes 13–17), cFANCD2(1-1167) (lanes 18–22), and cFANCD2(953-1439) (lanes 23–27) in the presence of wheat germ topoisomerase I. After deproteinization, the topoisomers were separated by agarose gel electrophoresis with ethidium bromide staining. The cFANCD2 concentrations were 0, 0.45, 0.90, and 1.8 μM. Highly supercoiled and relaxed DNAs are denoted as 'sc' and 'relaxed', respectively. (**D**) Graphic representation of nucleosome-assembly activities of the cFANCD2 mutants shown in **C**. Representative images are shown in **C**. The supercoiled DNA fractions were generated by nucleosome assembly in the presence of cFANCD2, and the intensities of the bands indicated by the arrows in **C** were quantitated by an LAS-4000 Image Analyser (GE Healthcare). Means of three independent experiments are shown with s.d.'s. (**E**) Nucleosomes were reconstituted on the relaxed plasmid DNA by cFANCD2 (lanes 3–7), cFANCD2(R1336A/K1346A) (lanes 8–12), and cFANCD2(D1350A/E1365A/E1382A) (lanes 13–17) in the presence of wheat germ topoisomerase I. The cFANCD2 concentrations were 0, 0.45, 0.90, and 1.8 μM. Highly supercoiled and relaxed DNAs are denoted as 'sc' and 'relaxed', respectively. (**F**) Graphical representation of the nucleosome-assembly activities of the cFANCD2 mutants shown in **E**. Representative images are shown in **E**. The supercoiled DNA fractions were generated by nucleosome assembly in the presence of cFANCD2, and the intensities of the bands indicated by the arrows in **E** were quantitated by an LAS-4000 Image Analyser (GE Healthcare). Means of three independent experiments are shown with s.d.'s.

FANCD2 mediates histone mobilization in living cells in a DNA damage-dependent manner

To determine whether FANCD2 plays a role in histone dynamics in living cells during DNA repair, we knocked down hFANCD2 in HeLa cells expressing histone H3-GFP (Kimura and Cook, 2001), using small inhibitory RNA (siRNA). Three days after the transfection of the specific siRNA, the level of hFANCD2 had decreased substantially, to <10% of the normal level (Supplementary Figure S4A and B). Using these cells, the mobility of H3 was analysed by fluorescence recovery after photobleaching (FRAP) (Kimura *et al*, 2006). The recovery kinetics (the curve shapes) of the exchanging fractions were similar in the hFANCD2-knockdown and control cells (Figure 3A), suggesting that hFANCD2 does not play a major role in H3 assembly or exchange under normal conditions. As FA-mutant cells display significant sensitivity to interstrand DNA crosslinking reagents, such as mitomycin C (MMC) (Niedernhofer *et al*, 2005; Thompson *et al*, 2005; Wang, 2007; Kee and D'Andrea, 2010; Garner and Smogorzewska, 2011; Kitao and Takata, 2011), we next tested the effect of MMC on the H3 mobility in the hFANCD2-knockdown HeLa cells. Interestingly, the recovery of H3-GFP in the hFANCD2-knockdown cells was clearly slower in the presence of MMC (Figure 3B). Similar results were obtained with a different FANCD2-specific siRNA (Supplementary Figure S4C). The slower H3-GFP exchange observed in the MMC-treated FANCD2-knockdown cells could be due to a different cell cycle distribution, since the FA-deficient cells may be arrested at S and/or G2 due to the deficiency of DNA crosslink repair. We therefore performed FRAP experiments in cells stably expressing both H3-GFP and mCherry-tagged PCNA, which shows characteristic patterns representing replication and repair foci (Leonhardt *et al*, 2000). We first examined the mobility of H3-GFP in different cell cycle stages under the normal growth conditions. The H3-GFP mobility in PCNA foci-positive (S-phase) cells did not differ from that in PCNA foci-negative cells (Figure 3C). In the presence of MMC, the PCNA foci-positive cells were indeed enriched by the hFANCD2 knockdown, but the mobility of H3-GFP was still slower than that in the MMC-treated PCNA foci-positive control cells (Figure 3D; Supplementary Figure S4D). Therefore, the reduced histone H3 mobility in the MMC-treated hFANCD2-knockdown cells does not appear to be attributable to a difference in the cell cycle phase. Furthermore, the slower H3-GFP recovery in the presence of MMC was also detected in the hFANCA-knockdown cells, in which the damage-dependent focus formation of hFANCD2 on chromosomes was significantly inhibited (Supplementary Figure S4E–H). These data suggest that hFANCD2 may mediate nucleosome assembly and/or histone exchange in human cells, in a damage-dependent manner.

The C-terminal histone-binding region of FANCD2 is important for the DNA repair mediated by the FA pathway

To determine whether the histone assembly activity levels of the FANCD2 mutants *in vitro* correlate with their DNA-repair activities *in vivo*, we expressed them in *FANCD2*$^{-/-}$ DT40 cells, and exposed the cells to cisplatin in a colony survival assay. As shown in Figure 4A, full-length cFANCD2, cFANCD2(1-1389), and cFANCD2(D1350A/E1365A/E1382A) rescued the cisplatin-sensitive phenotype of the *cFANCD2*$^{-/-}$ cells, in contrast to cFANCD2(1-1167), cFANCD2(1-1267),

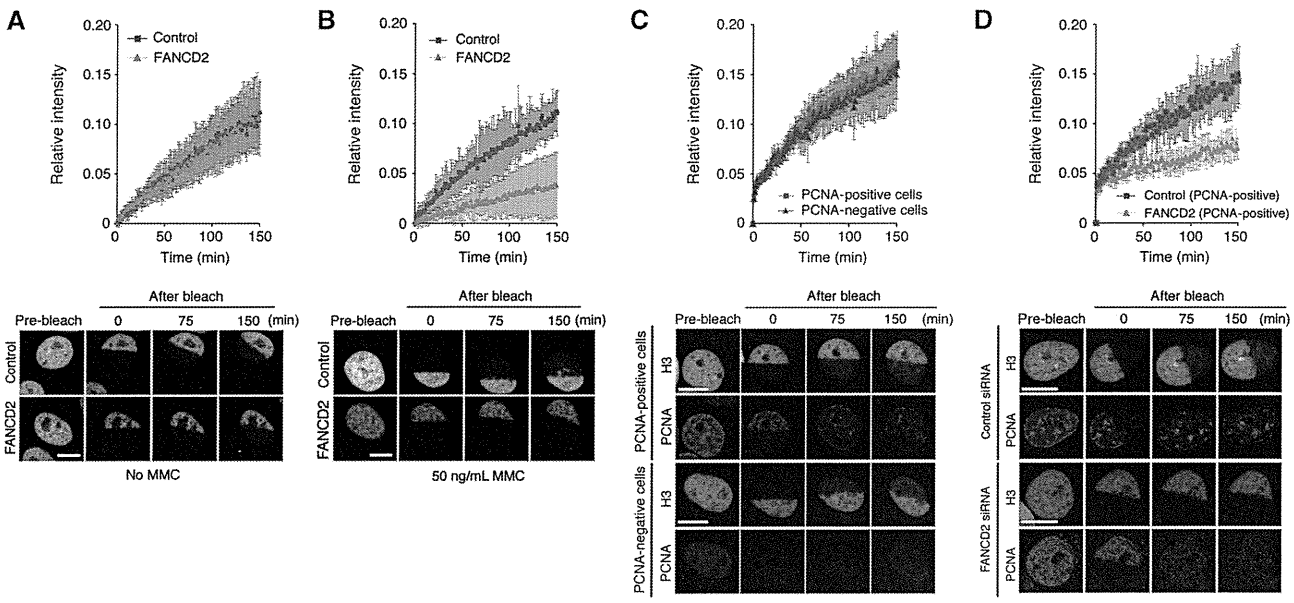

Figure 3 Histone H3 mobility is decreased in FANCD2-knockdown cells in the presence of a DNA crosslinking reagent. (**A**, **B**) FRAP with HeLa cells. Three days after the transfection of hFANCD2-siRNA or control RNA, the mobility of histone H3-GFP was analysed by bleaching one-half of a nucleus in the absence (**A**) or presence (**B**) of 50 ng/ml MMC for 12–18 h. The mean of the relative fluorescence intensity with the s.d. ($n = 10$–11) and examples are shown. (**C**) FRAP with HeLa cells stably expressing mCherry-PCNA. Three days after the transfection of control RNA, the mobility of histone H3-GFP was analysed in the absence of MMC. The PCNA foci-positive (S-phase) cells were identified by the characteristic mCherry-PCNA distribution. The mean of the relative fluorescence intensity with the s.d. ($n = 10$–14) and examples are shown. (**D**) FRAP with MMC-treated HeLa cells expressing H3-GFP and mCherry-PCNA in S-phase. Three days after the transfection of hFANCD2-siRNA or control RNA, the mobility of histone H3-GFP in the PCNA foci-positive (S-phase) cells was analysed in the presence of 50 ng/ml MMC. The mean of the relative fluorescence intensity with the s.d. ($n = 10$–18) and examples are shown. Bars: 10 μm.

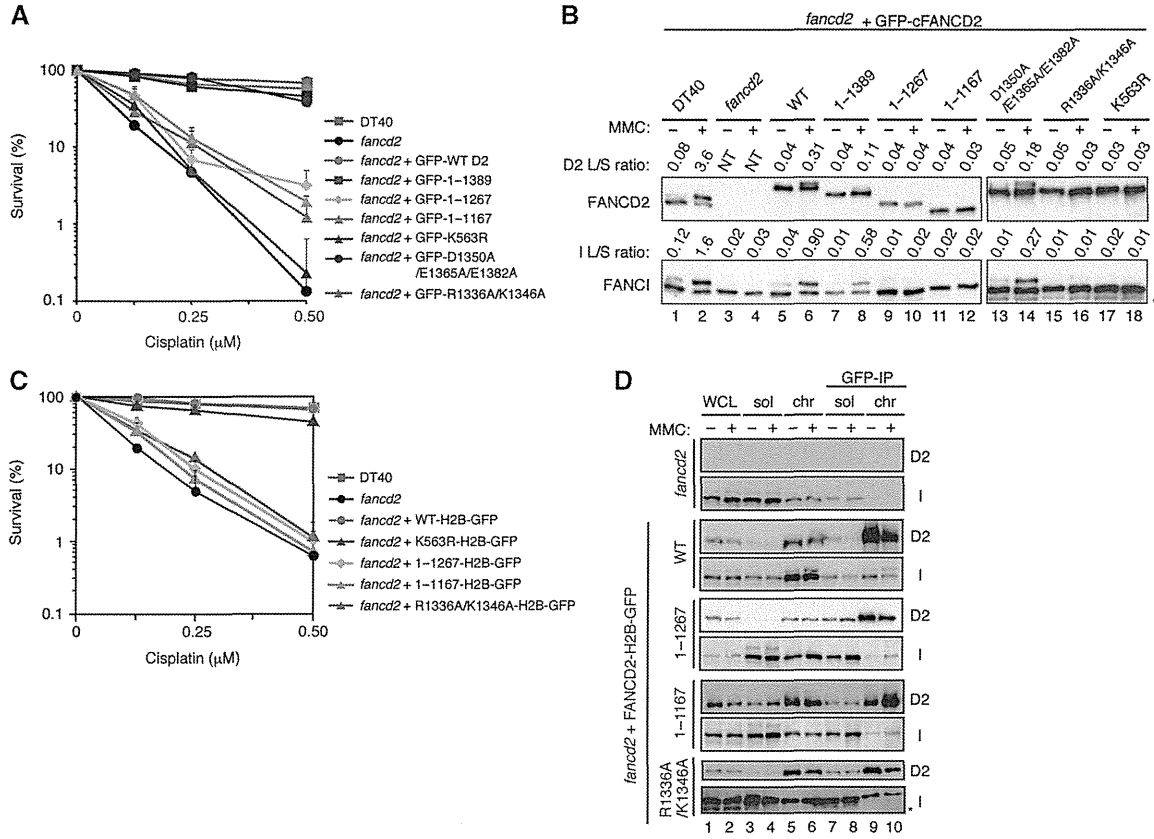

Figure 4 DNA-repair defects in the cFANCD2 C-terminal mutants. (**A**) Colony survival assay of the *cFANCD2*$^{-/-}$ DT40 cells expressing GFP fusions with the wild-type (WT) and indicated cFANCD2 mutants in the presence of cisplatin. The mean and s.d. of measurements performed in triplicate are shown. (**B**) FANCD2/FANCI monoubiquitination in *cFANCD2*$^{-/-}$ cells expressing the indicated cFANCD2 mutants. Cells were treated with or without MMC, and the WCEs were subjected to western blotting. The bands detected just above the original bands (S-forms) correspond to the monoubiquitinated forms (L-forms) of cFANCD2 and cFANCI (lanes 2, 6, 8, and 14). The L-form and S-form bands were quantitated with the Image J software, and the L/S ratios are indicated just above each panel. An asterisk indicates the non-specific bands. ND: not detectable. (**C**) Colony survival assay of the *cFANCD2*$^{-/-}$ cells expressing H2B-GFP fusions with the WT and indicated cFANCD2 mutants in the presence of cisplatin. The mean and s. d. of measurements performed in triplicate are shown. (**D**) Chromatin targeting of cFANCD2 (WT)-H2B, cFANCD2(1-1167)-H2B, cFANCD2(1-1267)-H2B, and cFANCD2(R1336A/K1346A)-H2B. Negative control experiments in the absence of exogenously expressed cFANCD2 are shown in the top panel. The *cFANCD2*$^{-/-}$ cells expressing the indicated proteins were treated with MMC (500 ng/ml, 6 h) or left untreated and then fractionated. Each fraction was separated by SDS–PAGE, and western blotting was performed using anti-cFANCD2 and anti-cFANCI antibodies. An asterisk indicates the non-specific band.

and cFANCD2(R1336A/K1346A). To ensure the chromatin targeting of these cFANCD2 mutants, we repeated this assay with the cFANCD2 mutants expressed as fusions with histone H2B, since cFANCD2(1-1167), cFANCD2(1-1267), and cFANCD2(R1336A/K1346A) were not monoubiquitinated (Figure 4B), probably due to the weakened interaction with FANCL, which was identified as the catalytic E3 subunit for FANCD2 monoubiquitination (Meetei *et al*, 2003) (Supplementary Figure S5A). We confirmed that the fusion of H2B to cFANCD2 and cFANCD2(1-1267) did not affect their nucleosome-assembly activities (Supplementary Figure S5B–E). Although substantial amounts of cFANCD2(1-1167)-H2B, cFANCD2(1-1267)-H2B, and cFANCD2(R1336A/K1346A)-H2B were detected at the chromatin (Figure 4D), the mutants still could not complement the cisplatin sensitivity of *cFANCD2*$^{-/-}$ cells, in contrast to the H2B fusion proteins with the full-length cFANCD2 and cFANCD2(K563R), bearing a point mutation at the monoubiquitination site (K563R) (Figure 4C) (Matsushita *et al*, 2005). These results strongly suggest that the nucleosome-assembly activity, which depends on the C-terminal region of FANCD2, might be crucial for the DNA repair mediated by the FA pathway. Notably, these cFANCD2 mutants were able to interact with the cFANCI protein in chromatin, as detected by anti-GFP immunoprecipitation followed by western blotting (Figure 4D), and as further supported by the results of *in vitro* binding experiments (Supplementary Figure S7F–H).

A disease-related FA mutant, human FANCD2(R302W), and its chicken counterpart, cFANCD2(R305W), are monoubiquitinated but do not facilitate histone exchange

As shown in Figure 4B, the C-terminally deleted or point FANCD2 mutants, which were defective in nucleosome assembly, were also defective in monoubiquitination, probably due to their weakened interactions with FANCL (Supplementary Figure S5A). This suggested that the histone-binding and FANCL-binding regions may partially overlap. To provide evidence that the FANCD2 histone-chaperone activity functions in DNA repair independently of its monoubiquitination, a FANCD2 mutant, in which the histone-chaperone and monoubiquitination activities are separated, would be useful.

We reasoned that such mutations might be found outside the putative histone-binding site. We found that the chicken FANCD2 R305W mutation (Arg305 to Trp), which corresponds to a disease-related mutation (human FANCD2 R302W) in FA (Timmers *et al*, 2001), is such a separation mutation. cFANCD2(R305W) exhibited reduced histone binding (Figure 2B, lane 8), and was defective in the nucleosome-assembly activity (Figure 5A and B). In contrast, cFANCD2(R305W) was proficient in its monoubiquitination (Figure 5C) and chromatin-targeting activities (Supplementary Figure S6A). Interestingly, cFANCD2(R305W) was moderately defective in the repair of DNA damage induced by cisplatin (Figure 5D), although its binding to cFANCI was proficient *in vivo* (Supplementary Figure S6A) and *in vitro* (Supplementary Figure S7E). The DNA-repair deficiency was also observed when H2B-fused cFANCD2(R305W) was expressed in the *cFANCD2*$^{-/-}$ cells (Figure 5E). These results indicated that the DNA-repair defect observed in the *cFANCD2*$^{-/-}$ cells expressing cFANCD2(R305W) may be accounted for by the defective histone chaperone activity of cFANCD2(R305W). Therefore, the histone chaperone activity of FANCD2 may be required in the steps after the FANCD2 monoubiquitination and chromatin targeting, during DNA repair by the FA pathway (Figure 8B).

To test whether the histone chaperone activity of FANCD2 functions in histone dynamics in living cells, we expressed mCherry-tagged hFANCD2, hFANCD2(R302W), or hFANCD2 (K561R) in H3-GFP-expressing HeLa cells, in which the endogenous hFANCD2 was knocked down by siRNA (Supplementary Figure S6B). We compared the H3-GFP mobility between mCherry-positive and -negative cells. The mobility of H3-GFP was efficiently restored with the expression of wild-type (WT) hFANCD2 (Figure 6A), but not with the monoubiquitination-deficient hFANCD2(K561R) mutant (Figure 6B, top panel), consistent with its chromatin-targeting deficiency (diffusing within the nucleus; Figure 6B, bottom panels). Interestingly, hFANCD2(R302W) also failed to restore the H3-GFP mobility (Figure 6C, top panel), although its chromatin targeting was not defective (forming nuclear foci like the WT hFANCD2; Figure 6C, bottom panels). Together with the DNA-repair deficiency of the *cFANCD2*$^{-/-}$ cells expressing cFANCD2(R305W), these results support the view that the histone-chaperone activity of FANCD2 is important in the DNA repair by the FA pathway. It should be noted that the VU008 patient cell line, which has the hFANCD2(R302W) mutation, produces the mutant hFANCD2 protein at extremely low levels (Timmers *et al*, 2001). Therefore, both defective histone-chaperone activity

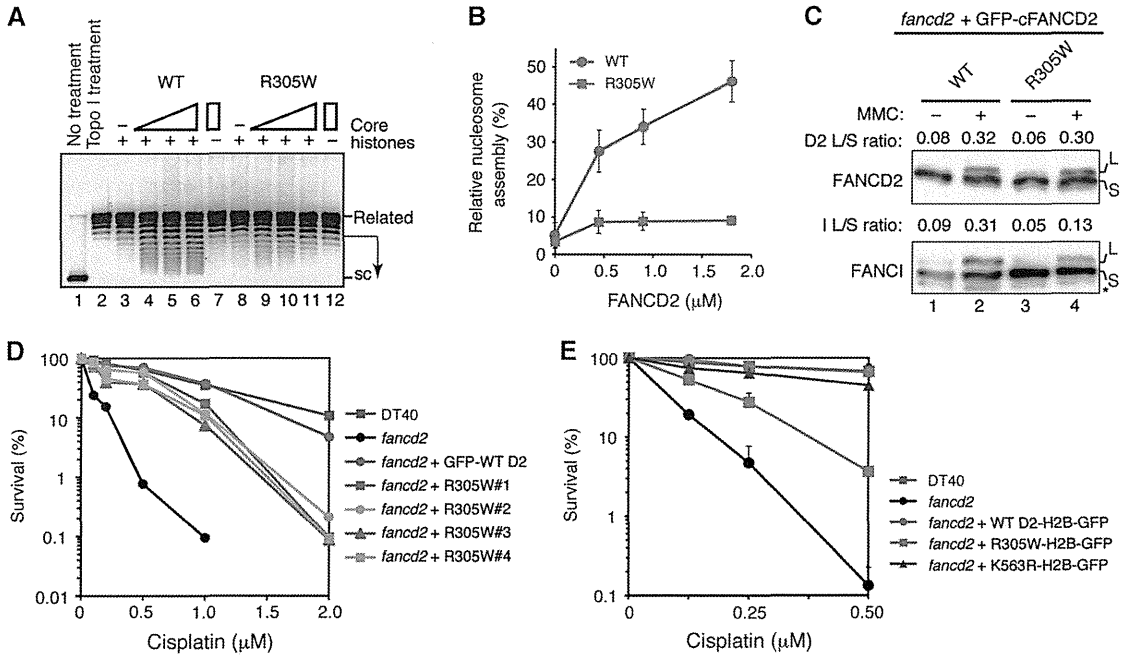

Figure 5 An FA-related mutant, cFANCD2(R305W), is defective in nucleosome-assembly activity and DNA repair. (**A**) Nucleosomes were reconstituted on the relaxed plasmid DNA by cFANCD2 (lanes 3–7) and cFANCD2(R305W) (lanes 8–12), in the presence of wheat germ topoisomerase I. After deproteinization, the topoisomers were separated by agarose gel electrophoresis. The cFANCD2 concentrations were 0, 0.45, 0.90, and 1.8 μM. Highly supercoiled and relaxed DNAs are denoted as 'sc' and 'relaxed', respectively. (**B**) Graphical representation of the nucleosome-assembly activity of the cFANCD2(R305W) mutants. Representative images are shown in **A**. The supercoiled DNA fractions were generated by nucleosome assembly in the presence of cFANCD2 (indicated by arrows in **A**), and the intensities of the bands indicated by the arrows in **A** were quantitated by an LAS-4000 Image Analyser (GE Healthcare). Means of three independent experiments are shown with s.d.'s. (**C**) FANCD2/FANCI monoubiquitination in *cFANCD2*$^{-/-}$ cells expressing the wild-type (WT) FANCD2 or cFANCD2(R305W). Cells were treated with or without MMC, and the WCEs were subjected to western blotting. The bands detected just above the original bands (S-forms) correspond to the monoubiquitinated forms (L-forms) of cFANCD2 and cFANCI (lanes 2 and 4). The L-form and S-form bands were quantitated with the Image J software, and the L/S ratios are indicated just above each panel. An asterisk indicates the non-specific band. (**D**) Colony survival assay of the cFANCD DT40 cells expressing GFP fusions with the wild type (WT) and cFANCD2(R305W), in the presence of cisplatin. Four independent DT40 cells expressing cFANCD2(R305W) were tested and plotted. (**E**) Colony survival assay of the *cFANCD2*$^{-/-}$ DT40 cells expressing H2B–GFP fusions with the WT and cFANCD2(R305W), in the presence of cisplatin. The mean and s.d. of measurements performed in triplicate are shown.

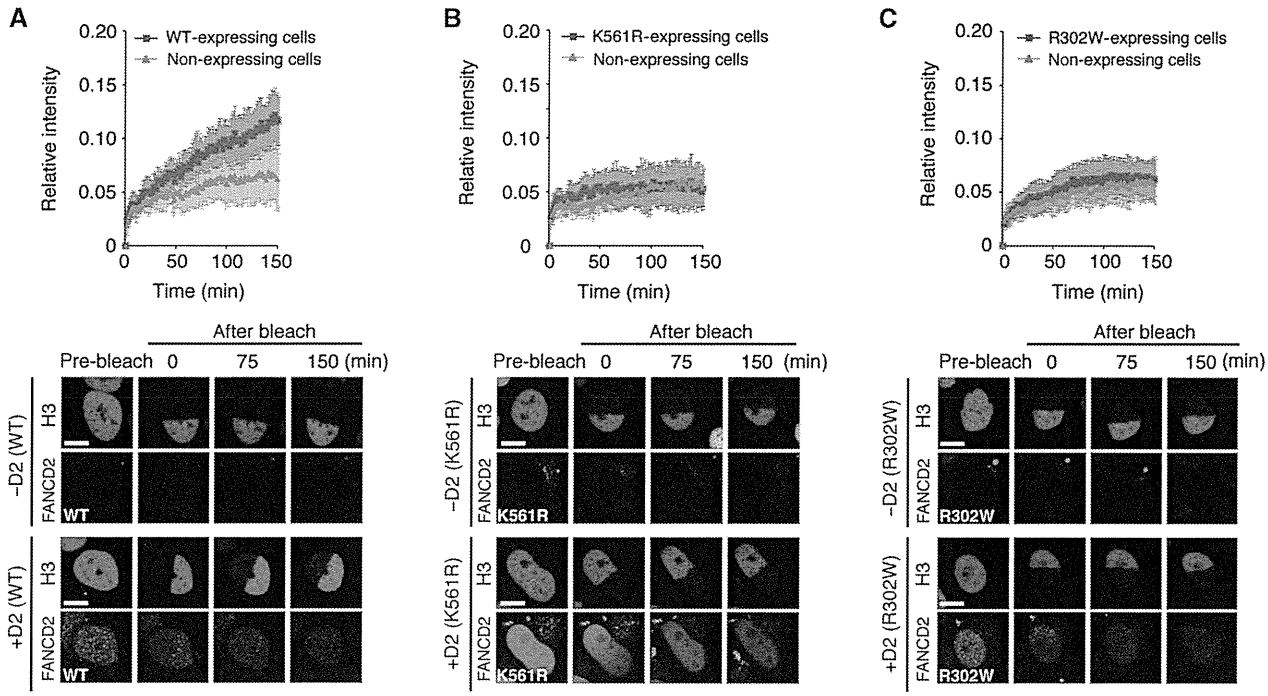

Figure 6 An FA-related mutant, human FANCD2(R302W), is defective in facilitating histone exchange. (**A**–**C**) FRAP with HeLa cells expressing H3-GFP and mCherry fusions with hFANCD2 (WT) (**A**), hFANCD2(K561R) (**B**), and hFANCD2(R302W) (**C**). After the depletion of endogenous hFANCD2 by siRNA, mCherry-hFANCD2, hFANCD2(K561R), or -hFANCD2(R302W) was expressed. In these cells, the mobility of histone H3-GFP was analysed in the presence of 50 ng/ml MMC for 12–18 h. The mean of the relative fluorescence intensity with the s.d. ($n = 10$–12) and examples are shown. Bars: 10 μm.

and instability of hFANCD2(R302W) protein may be potential causes of the FA phenotype in this patient.

FANCI stimulates nucleosome assembly by FANCD2

Finally, we examined the involvement of FANCI in nucleosome assembly, using purified chicken FANCI (cFANCI) (Supplementary Figure S7A and B), which could form a stable complex with cFANCD2 (Figure 7A). Although FANCI shares significant homology with FANCD2 (Sims *et al*, 2007; Smogorzewska *et al*, 2007), purified cFANCI alone did not efficiently promote nucleosome assembly (Figure 7B). However, cFANCI clearly stimulated the cFANCD2-mediated nucleosome assembly at low cFANCD2 concentrations, at which cFANCD2 itself did not promote detectable levels of nucleosome assembly (Figure 7C and D). cFANCI did not form a complex with the major histone chaperone Nap1, and did not stimulate its nucleosome assembly (Supplementary Figure S7C and D), suggesting that it may specifically stimulate the cFANCD2-mediated nucleosome assembly. In addition, cFANCI stimulated the nucleosome-assembly activity of cFANCD2(1-1389), which retained H3/H4-binding ability, but not that of cFANCD2(1-1267) (Supplementary Figure S7I). Therefore, the ID complex may facilitate nucleosome reorganization during DNA repair.

Discussion

In the present study, we found that the purified FANCD2 protein promotes nucleosome assembly *in vitro*, and that its partner, FANCI, significantly stimulates this activity. We also discovered that the C-terminal region of FANCD2 is critical for the nucleosome-assembly activity, and showed that the FANCD2 deletion and point mutants are defective in both nucleosome assembly *in vitro* and tolerance to cisplatin treatment *in vivo*. These findings provide novel insights into the function of the ID complex in chromatin.

The crystal structure of the mouse ID complex revealed that FANCD2 is composed of seven subdomains, solenoid 1 (S1), helical domain 1 (HD1), solenoid 2 (S2), helical domain 2 (HD2), solenoid 3 (S3), solenoid 4 (S4), and the C-terminal acidic region (Joo *et al*, 2011). In the present study, we mapped the histone-binding region within the S4 domain of FANCD2. The FANCD2 S4 domain is separate from the FANCI-binding surface, and is largely accessible (Joo *et al*, 2011). In the S4 domain, the cFANCD2 Arg1336 and Lys1346 residues are perfectly conserved among the human, mouse, chicken, frog, fish, and fly FANCD2 proteins (Figure 2A), and are located on the concave surface (Figure 8A; Joo *et al*, 2011). Our mutational analysis revealed that the cFANCD2 Arg1336 and Lys1346 residues are essential for nucleosome assembly *in vitro* and cisplatin resistance *in vivo*. In the crystal structure, the side chains of the mouse FANCD2 Arg1334 and Lys1344 residues, corresponding to the cFANCD2 Arg1336 and Lys1346 residues, respectively, are completely exposed to the solvent on the concave surface (Figure 8A). Therefore, the concave surface of the FANCD2 S4 domain may be its histone-binding region.

In cFANCD2, Arg1336 and Lys1346 are positively charged residues, which are considered to be less important for the histone binding of the acidic histone chaperone, Asf1 (English *et al*, 2006; Natsume *et al*, 2007). However, the involvement of positively charged residues in histone

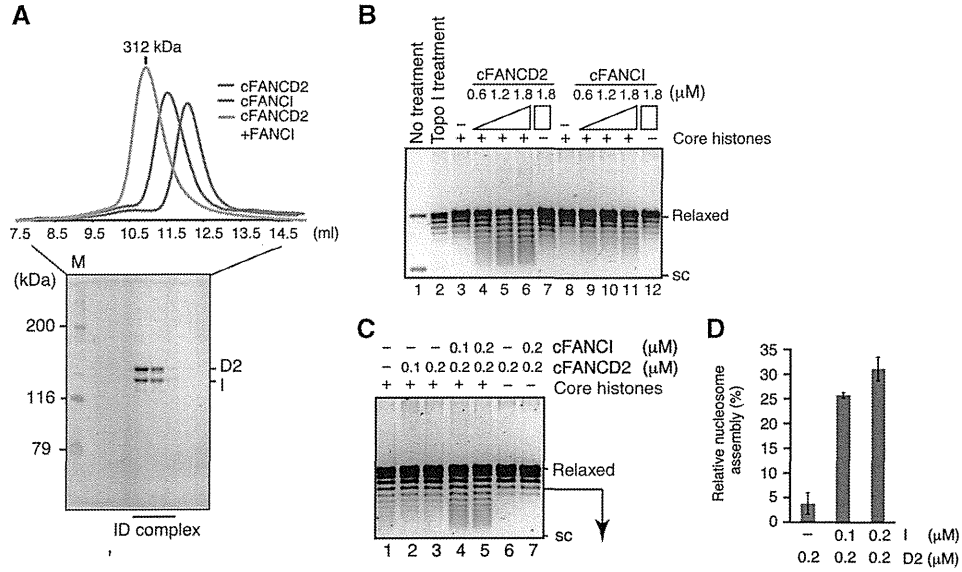

Figure 7 FANCI stimulates the FANCD2-mediated nucleosome assembly. (**A**) Gel filtration analysis of cFANCI–cFANCD2 complex formation. The SDS–PAGE analysis of the cFANCI–cFANCD2 fractions is shown below the gel filtration profiles. (**B**, **C**) Nucleosomes were reconstituted with relaxed plasmid DNA and cFANCD2 and/or cFANCI in the presence of wheat germ topoisomerase I. After deproteinization, the topoisomers were separated by agarose gel electrophoresis. The protein concentrations used in the assay are indicated at the top of the panels. Highly supercoiled and relaxed DNAs are denoted as 'sc' and 'relaxed', respectively. (**D**) Graphical representation of the experiments shown in **C**, lanes 3–5. The supercoiled DNA fractions generated by nucleosome assembly in the presence of cFANCD2 and cFANCI (indicated by arrows in **C**) were quantitated. Means of three independent experiments are shown with s.d.'s.

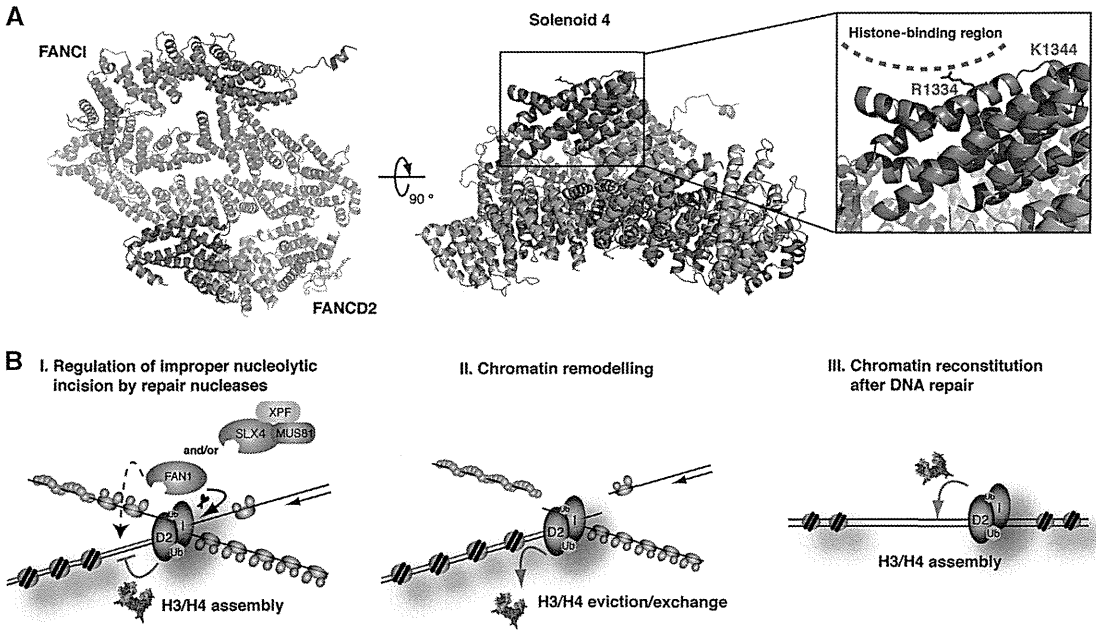

Figure 8 Models for the FANCD2 function in the FA pathway. (**A**) Locations of the Arg1334 and Lys1344 residues in the mouse FANCD2 structure. Structure of the mouse ID complex (PDB ID: 3S4W; Joo *et al*, 2011). The FANCD2 and FANCI subunits are coloured grey and light blue, respectively. The FANCD2 Arg1334 and Lys1344 residues (red), corresponding to the cFANCD2 Arg1336 and Lys1346 residues, respectively, are located on the concave surface of the FANCD2 Solenoid 4 (S4) domain (dark grey). (**B**) Three possible functions of the histone chaperone activity of the ID complex. (I) After the chromatin binding and monoubiquitination of the ID complex, the nucleosomes assembled by the ID complex on newly synthesized DNA may suppress the improper nucleolytic digestion by the repair nucleases, such as FAN1 and the SLX4 nuclease complex, which are recruited by the monoubiquitinated ID complex. (II) Chromatin remodelling mediated by the ID complex and FANCD2-associated chromatin modifiers may facilitate the RAD51-mediated homologous recombination reaction in chromatin. (III) The nucleosome-assembly activity of the ID complex may be required for chromatin reconstitution after DNA repair. RAD51 and RPA are coloured red and green, respectively. Histone octamers are shown in brown.

binding has been reported in the histone chaperone HJURP, which is the specific chaperone for the histone H3 variant, CENP-A (Dunleavy *et al*, 2009; Foltz *et al*, 2009). In the complex of HJURP with histone H4 and CENP-A, polar interactions exist between the negatively charged Glu96 of CENP-A and the two positively charged Arg32 and Lys39

residues of HJURP, and also between Glu107 of CENP-A and Arg28 of HJURP (Hu *et al*, 2011). Interestingly, the Glu96 and Glu107 residues of CENP-A are both conserved in histone H3 (Tachiwana *et al*, 2011a). Therefore, the histone-binding mechanism of FANCD2 may be similar to that of HJURP.

In the present study, we found that cFANCD2(R305W) was clearly defective in reversing the cisplatin sensitivity of the *FANCD2*$^{-/-}$ DT40 cells, but was proficient in its monoubiquitination *in vivo*. Interestingly, cFANCD2(R305W) was significantly defective in both the histone-binding and nucleosome-assembly activities. In addition, the corresponding human FANCD2(R302W) mutant could not rescue the decreased histone H3 mobility in the FANCD2-knockdown cells. These findings indicate that the histone-chaperone activity of FANCD2 is actually involved in the DNA crosslink repair by the FA pathway, and strongly suggest that FANCD2 regulates nucleosome dynamics after its monoubiquitination. The C-terminal cFANCD2 mutants tested in this study showed more severe cisplatin sensitivity than cFANCD2(R305W), even when localized in the chromatin by the H2B fusion. The residual histone-chaperone activity of cFANCD2 (R305W), which was barely detectable in the present nucleosome formation assay, may partially complement the cisplatin sensitivity of the *cFANCD2*$^{-/-}$ cells. In the crystal structure of mouse FANCD2, the side chain of the corresponding Arg300 directly hydrogen bonds with Asp379 (Joo *et al*, 2011), suggesting that the Arg300–Asp379 interaction may be important in the tertiary structure of the protein. Therefore, the Arg to Trp substitution found in cFANCD2(R305W) or hFANCD2(R302W) may cause a large structural change, which may allosterically impair the histone-binding activity of FANCD2.

FANCI–FANCD2 is reportedly required for nucleolytic incisions in a replicating plasmid carrying an interstrand crosslink in a frog egg extract (Knipscheer *et al*, 2009). One can envision that the ID complex-mediated chromatin remodelling may regulate the incision step by promoting the recruitment of nucleases (Figure 8B, I) (e.g., FAN1, Mus81, and XPF) (Nomura *et al*, 2007; Bhagwat *et al*, 2009; Fekairi *et al*, 2009; Svendsen *et al*, 2009; Hicks *et al*, 2010; Kratz *et al*, 2010; MacKay *et al*, 2010; Smogorzewska *et al*, 2010; Yoshikiyo *et al*, 2010; Yamamoto *et al*, 2011). In this step, the proper incision by the repair nucleases may occur on the single-stranded DNA region (Figure 8B, I, arrowhead), while the improper digestion of intact DNA strands may be restricted by the nucleosomes formed by the ID complex (Figure 8B, I, dashed line). Second, in the FA pathway, homologous recombination repair may be promoted after FANCD2 assembly into chromatin. The nucleosome remodelling by the ID complex may facilitate the DNA recombination reaction mediated by RAD51, which is the key protein for homologous recombinational repair (Figure 8B, II). Finally, the histone assembly activity of the ID complex may simply be important for chromatin reformation, following crosslink removal and DNA repair (Figure 8B, III). In addition to the direct interaction of the ID complex with histones, presented here, several chromatin modifiers have been suggested to interact with FA proteins. For example, a histone acetyltransferase, TIP60, reportedly interacts with FANCD2 (Hejna *et al*, 2008). Thus, the function of FANCD2 may be tightly coupled with those of other chromatin remodelling factors in chromatin dynamics, to facilitate DNA crosslink repair.

Materials and methods

Purifications of FANCD2, FANCI, FANCL, UBE2T, and Nap1

Experimental procedures are described in Supplementary Materials and Methods. The protein concentration was determined by the Bradford method (Bradford, 1976), using bovine serum albumin as the standard protein.

Purification of recombinant human H3/H4 and H2A/H2B complexes

Human histones H2A, H2B, H3, and H4 were overexpressed in *Escherichia coli* cells as His_6-tagged proteins, as described (Tanaka *et al*, 2004; Tachiwana *et al*, 2008). The purification and preparation of the histone H3/H4 and H2A/H2B complexes were performed as previously described (Tachiwana *et al*, 2010, 2011b). The His_6-tag was removed during the purification steps.

Proteome analysis

The purified recombinant human histone H3/H4 complex was covalently conjugated with Affi-Gel 10 beads (Bio-Rad), according to the manufacturer's protocol. Briefly, the histone H3/H4 beads were incubated with a chromatin extract from HeLa cells at 4°C. The beads were washed with 10 mM PIPES buffer (pH 7.0), containing 1 mM $MgCl_2$, 1 mM EDTA, 0.01% Triton X-100, 300 mM sucrose, and 0.1 M NaCl. The proteins bound to the beads were fractionated by SDS–PAGE. Each lane was cut into nine pieces, and was further treated with trypsin. To identify the peptide fragments, the samples were analysed by liquid chromatography/tandem mass spectrometry, as previously described (Nozawa *et al*, 2010). The raw data files were analysed by the Mascot software (Matrix Science).

Pull-down assay with histone-conjugated beads

The histone H3/H4 complex was covalently conjugated with Affi-Gel 10 beads (Bio-Rad), according to the manufacturer's protocol. The histone H3/H4 beads were incubated with a HeLa whole-cell extract (WCE) (3 mg of protein), and the beads were washed three times with 100 µl of washing buffer, containing 50 mM Tris–HCl (pH 7.5), 200 mM NaCl, 5 mM EDTA, 0.5% Nonidet P-40, 1 mM PMSF, and Protease Inhibitor Cocktail (Nacalai Tesque). The hFANCD2 that copelleted with the histone H3/H4 beads was fractionated by 8% SDS–PAGE, and was detected by western blotting with the hFANCD2-specific mouse monoclonal antibody (FI17, Santa Cruz Biotechnology, Inc.).

For the recombinant hFANCD2-binding assay, the histone H3/H4 beads (15 µl) were incubated with purified hFANCD2, with or without 10 U of DNaseI (TOYOBO), at 23°C for 120 min. The beads were then washed three times with 100 µl of 10 mM PIPES-KOH buffer (pH 7.0), containing 0.5 M NaCl, 0.3 M sucrose, 1 mM $MgCl_2$, and 0.01% Triton X-100. The proteins bound to the beads were separated by 15% SDS–PAGE, and were visualized by Coomassie Brilliant Blue staining.

For the cFANCD2-binding assay, 293T cells were transiently transfected with GFP-cFANCD2-mutant plasmids, using Lipofectamine2000 (Invitrogen). Cells were disrupted in lysis buffer (Seki *et al*, 2007), and after the lysate was incubated with the histone H3/H4 beads (7.5 µl) at 4°C for 3 h, the beads were washed four times with lysis buffer. The proteins were separated by 6% SDS–PAGE, and were detected by western blotting with an anti-GFP Ab (Clontech).

Topological assay for nucleosome formation

Experimental procedures are described in Supplementary Materials and Methods.

Gel-shift assay for nucleosome formation

The H2A/H2B complex (8 ng/µl) and the H3/H4 complex (8 ng/µl) were pre-incubated with hFANCD2 or hNap1 at 23°C for 10 min. The nucleosome-assembly reaction was initiated by the addition of the 195 bp DNA (8 ng/µl) containing the *Lytechinus variegates* 5S ribosomal RNA gene (Osakabe *et al*, 2010) in a 10 µl reaction mixture, containing 20 mM Tris–HCl (pH 8.0), 140 mM NaCl, 7% glycerol, and 1 mM dithiothreitol. The reaction was continued at 23°C for 60 min, followed by a further incubation at 42°C for 60 min to eliminate the non-specific DNA binding by free histones. The samples were then separated by 6% PAGE in 0.2× TBE buffer

(18 mM Tris base, 18 mM boric acid, and 0.4 mM EDTA). DNA was visualized by ethidium bromide staining.

Pull-down assay with GST-cFANCL and cFANCD2

Purified cFANCD2 (6 μg) and GST-cFANCL (5 μg) were incubated at 30°C for 60 min in a 100 μl reaction mixture, containing 20 mM Tris–HCl (pH 8.0), 10% glycerol, 200 mM NaCl, and 5 mM 2-mercaptoethanol. Glutathione Sepharose 4B beads (5 μl) were added to the reaction mixtures, which were gently mixed at 4°C for 60 min. The beads were then washed three times with 1 ml of wash buffer, containing 20 mM Tris–HCl (pH 8.0), 0.4 M NaCl, 10% glycerol, 5 mM 2-mercaptoethanol, and 0.05% Triton X-100. The proteins bound to the beads were separated by 7% SDS–PAGE, and were visualized by Coomassie Brilliant Blue staining.

In vitro FANCD2 monoubiquitination and purification of monoubiquitinated FANCD2

Experimental procedures are described in Supplementary Materials and Methods.

Gel-shift assay

Circular ϕX174 dsDNA (100 ng) was mixed with cFANCD2 (0.45–1.8 μM) or cFANCD2(1-1389) (0.45–1.8 μM) in 10 μl of reaction buffer, containing 22 mM Tris–HCl (pH 8.0), 70 mM NaCl, 7% glycerol, 2 mM $MgCl_2$, and 2.5 mM dithiothreitol. The samples were incubated at 37°C for 15 min, and were then analysed by 0.8% agarose gel electrophoresis in TAE buffer. DNA was visualized by ethidium bromide staining.

siRNA transfection, immunoblotting, and FRAP

The FANCD2-specific Stealth RNAs ((no. 1, HSS103525, 5′-AAUG AACGCUCUUUAGCAGACAUGG-3′, for Figures 3 and 6, and Supplementary Figure S3; and no. 2, HSS103527, 5′-AAUAGA CGACAACUUAUCCAUCACC-3′, for Supplementary Figure S3; Invitrogen), a FANCA-specific Stealth RNA (5′-AAGGGUCAAG AGGGAAAAAUA-3′, for Supplementary Figure S4; Invitrogen), and the control RNA (Negative Control Medium; Invitrogen) were introduced into HeLa cells expressing histone H3-GFP by Lipofectamine2000 (Invitrogen), as described (Kimura *et al*, 2006). Total cellular proteins were prepared 0–4 days after the RNA introduction, separated by 8% SDS–PAGE, and immunoblotted with a mouse monoclonal antibody directed against either FANCD2 (1:250; FI17, Santa Cruz Biotechnology, Inc.), α-tubulin (1:1000; Sigma) as a loading control, or an antibody against FANCA (1:1000; rabbit polyclonal, Bethyl Laboratories, Inc.). Secondary detection was performed with a sheep anti-mouse IgG, horseradish peroxidase-linked species-specific $F(ab')_2$ fragment (GE Healthcare; 1:500 for FANCD2 and 1:1000 for α-tubulin), or a sheep anti-rabbit IgG, horseradish peroxidase-linked species-specific $F(ab')_2$ fragment (GE Healthcare; 1:1000 for FANCA). The signals were detected by chemiluminescence (Western Lightning Plus; Perkin Elmer).

To generate HeLa cells expressing both H3-GFP and mCherry-PCNA, cells expressing H3-GFP (blasticidin resistance; Kimura and Cook, 2001) and mCherry-PCNA (puromycin resistance; generated using pMX-puro-based expression vector carrying mCherry-PCNA; Leonhardt *et al*, 2000; Kitamura *et al*, 2003) were fused using polyethylene glycol (Roche; Kimura and Cook, 2001), and single colonies were selected in the presence of 1 μg/ml blasticidin and 0.5 μg/ml puromycin.

FRAP was performed 3–4 days after siRNA transfection as described (Kimura *et al*, 2006), using a confocal microscope (FV-1000; Olympus) with a ×60 UPlanSApo NA = 1.35 lens. Three confocal images of a field containing 4–10 nuclei were collected (800 × 800 pixels, zoom 3, scan speed 2 μs/pixel, pinhole 800 μm, Kalman filtration for four scans, LP505 emission filter, and 0.1% transmission of 488-nm Ar laser), one half of each nucleus was bleached using 75% transmission of 488 nm and 100% of 514 nm (two iterations), and images were obtained using the original setting at 1 min intervals.

For the complementation experiments, RNAi-resistant *hFANCD2* genes were constructed by introducing silent mutations in the FANCD2-specific Stealth RNA (no. 1) target sequence (5′-TCTGCTAAAGAG-3′) as follows: 5′-TCCGCCAAGGAA-3′. HeLa cells expressing histone H3-GFP were transfected with the FANCD2-specific Stealth RNAs (no. 1) to knockdown the endogenous hFANCD2. The next day, the cells were transfected with the RNAi-resistant mCherry-*hFANCD2*, mCherry-*hFANCD2(R302W)*, or mCherry-*hFANCD2(K561R)* gene, using the FuGENE system (Promega), and were further grown for 2 days before FRAP. After FRAP, the glass-bottom dish was processed for immunofluorescence.

The fluorescence intensity of the bleached area was measured using Image J 1.39u (W Rasband; http://rsb.info.nih.gov/ij/). After subtracting the background, the intensity was normalized to the initial intensity before bleaching.

Immunofluorescence

For immunofluorescence, HeLa cells expressing histone H3-GFP were grown on a glass-bottom dish (Mat-tek), transfected with Stealth RNA, and fixed with 4% paraformaldehyde at 3 days after transfection. The fixed cells were permeabilized and stained using mouse anti-FANCD2 (1:250) and goat Cy3-conjugated anti-mouse IgG (1:500; Jackson Immunoresearch). When mCherry-*hFANCD2* was transfected, goat Cy5-conjugated anti-mouse IgG (1:500; Jackson Immunoresearch) was used as the secondary antibody. For double staining with FANCA, rabbit anti-FANCA (1:100; Bethyl Laboratories, Inc.) and goat Cy5-conjugated anti-rabbit IgG (1:500; Jackson Immunoresearch) are also used. DNA was counterstained with DAPI. The fluorescence images were obtained using a confocal microscope (Olympus FV-1000 with a ×60 UPlanSApo NA = 1.35 oil-immersion objective lens; or Carl Zeiss LSM510 with a ×40 C-Apo NA = 1.2 water-immersion objective lens).

Generation of the FANCD2$^{-/-}$ DT40 cells producing the FANCD2 mutants

Plasmids for the cFANCD2-mutant fusions were constructed in the pcDNA3.1-based GFP or histone H2B-GFP expression vector, by inserting FANCD2 fragments using the Gateway system (Invitrogen). To obtain stably expressing clones, these plasmids were transfected into *FANCD2*-deficient DT40 cells (Yamamoto *et al*, 2005), and the clones expressing the fusions were identified by measuring the GFP fluorescence with a FACSCalibur (Becton Dickinson), as described (Yamamoto *et al*, 2003; Ishiai *et al*, 2004).

Cisplatin sensitivity assay

Sensitivity to cisplatin (Nihon-Kayaku) was assayed by colony formation, in medium containing 1.4% methylcellulose and the indicated dosage of cisplatin (Yamamoto *et al*, 2003; Ishiai *et al*, 2004).

Cell fractionation and detection of FANCD2/FANCI proteins

The indicated cells were either treated with MMC (500 ng/ml for 6 h) or left untreated, and were fractionated into soluble and chromatin fractions, as described previously (Matsushita *et al*, 2005; Ishiai *et al*, 2008). Pull-down assays of cFANCD2-H2B-GFP proteins were performed using anti-GFP beads (MBL). The proteins were separated by 6% SDS–PAGE, and were detected by western blotting. The anti-chicken FANCD2 and FANCI antibodies were obtained by immunizing rabbits with the bacterially expressed His fusion protein with full-length chicken FANCD2 and the GST fusion protein with chicken FANCI (amino acids 1–251), respectively.

Gel filtration analysis

The purified cFANCD2 and cFANCI proteins were analysed by Superdex 200 HR 10/30 (GE Healthcare) gel filtration chromatography. The elution buffer contained 20 mM Tris–HCl (pH 8.0), 200 mM NaCl, 10% glycerol, and 1 mM DTT.

Supplementary data

Supplementary data are available at *The EMBO Journal* Online (http://www.embojournal.org).

Acknowledgements

We would like to thank Emi Uchida for expert technical assistance, and M Cristina Cardoso, Toshio Kitamura, and Shin-ya Isobe for materials. This work was supported in part by Grants-in-Aid from the Japanese Society for the Promotion of Science (JSPS), and the Ministry of Education, Culture, Sports, Science and Technology (MEXT), Japan. H Kurumizaka was also supported by the Waseda Research Institute for Science and Engineering, the Sagawa Foundation for Promotion of Cancer Research, and NOVARTIS